NAVAL POSTGRADUATE SCHOOL
Monterey, California

THESIS

A NUMERICAL INVESTIGATION OF MESOSCALE PREDICTABILITY

by

Jodi C. Beattie

March 2003

Thesis Advisor Wendell A. Nuss
Co-Advisor David S. Brown

Approved for public release; distribution unlimited

THIS PAGE INTENTIONALLY LEFT BLANK

REPORT DOCUMENTATION PAGE

Form Approved OMB No. 0704-0188

1. AGENCY USE ONLY ***(Leave blank)***	**2. REPORT DATE** March 2003	**3. REPORT TYPE AND DATES COVERED** Master's Thesis

4. TITLE AND SUBTITLE A Numerical Investigation of Mesoscale Predictability

5. FUNDING NUMBERS

6. AUTHOR (S) Beattie, Jodi C.

7. PERFORMING ORGANIZATION NAME(S) AND ADDRESS(ES)
Naval Postgraduate School
Monterey, CA 93943-5000

8. PERFORMING ORGANIZATION REPORT NUMBER

9. SPONSORING / MONITORING AGENCY NAME(S) AND ADDRESS(ES)

10. SPONSORING/MONITORING AGENCY REPORT NUMBER

11. SUPPLEMENTARY NOTES The views expressed in this thesis are those of the author and do not reflect the official policy or position of the U.S. Department of Defense or the U.S. Government.

12a. DISTRIBUTION / AVAILABILITY STATEMENT
Approved for public release; distribution is unlimited

12b. DISTRIBUTION CODE

13. ABSTRACT ***(maximum 200 words)***

As mesoscale models increase in resolution there is a greater need to understand predictability on smaller scales. The predictability of a model is related to forecast skill. It is possible that the uncertainty of one scale of motion can affect the other scales due to the nonlinearity of the atmosphere. Some suggest that topography is one factor that can lead to an increase of forecast skill and therefore predictability.

This study examines the uncertainty of a mesoscale model and attempts to characterize the predictability of the wind field. The data collected is from the summer, when the synoptic forcing is relatively benign. Mesoscale Model 5 (MM5) lagged forecasts are used to create a three-member ensemble over a 12-hour forecast cycle. The differences in these forecasts are used to determine the spread of the wind field. Results show that some mesoscale features have high uncertainty and others have low uncertainty, shedding light on the potential predictability of these features with a mesoscale model.

Results indicate that topography is a large source of uncertainty. This is seen in all data sets, contrary to other studies. The ability of the model to properly forecast the diurnal cycle also impacted substantially on the character and evolution of forecast spread. The persistent mesoscale features were represented reasonably well, however the detailed structure of these features had a fair amount of uncertainty.

14. SUBJECT TERMS Mesoscale modeling, Model Verification, Predictability, MM5			**15. NUMBER OF PAGES** 95
			16. PRICE CODE
17. SECURITY CLASSIFICATION OF REPORT Unclassified	**18. SECURITY CLASSIFICATION OF THIS PAGE** Unclassified	**19. SECURITY CLASSIFICATION OF ABSTRACT** Unclassified	**20. LIMITATION OF ABSTRACT** UL

NSN 7540-01-280-5500 **Standard Form 298 (Rev. 2-89)**
Prescribed by ANSI Std. 239-18

THIS PAGE INTENTIONALLY LEFT BLANK

Approved for public release; distribution is unlimited

A NUMERICAL INVESTIGATION OF MESOSCALE PREDICTABILITY

Jodi C. Beattie
Lieutenant Junior Grade, United States Navy
B.S., United States Naval Academy, 1999

Submitted in partial fulfillment of the
requirements for the degree of

MASTER OF SCIENCE IN METEOROLOGY AND PHYSICAL OCEANOGRAPHY

from the

NAVAL POSTGRADUATE SCHOOL
March 2003

Author: Jodi C. Beattie

Approved by: Wendell A. Nuss
Thesis Advisor

LCDR David S. Brown
Second Reader

Carlyle H. Wash
Chairman,Department of Meteorology

THIS PAGE INTENTIONALLY LEFT BLANK

ABSTRACT

As mesoscale models increase in resolution there is a greater need to understand predictability on smaller scales. The predictability of a model is related to forecast skill. It is possible that the uncertainty of one scale of motion can affect the other scales due to the nonlinearity of the atmosphere. Some suggest that topography is one factor that can lead to an increase of forecast skill and therefore predictability.

This study examines the uncertainty of a mesoscale model and attempts to characterize the predictability of the wind field. The data collected is from the summer, when the synoptic forcing is relatively benign. Mesoscale Model 5 (MM5) lagged forecasts are used to create a three-member ensemble over a 12-hour forecast cycle. The differences in these forecasts are used to determine the spread of the wind field. Results show that some mesoscale features have high uncertainty and others have low uncertainty, shedding light on the potential predictability of these features with a mesoscale model.

Results indicate that topography is a large source of uncertainty. This is seen in all data sets, contrary to other studies. The ability of the model to properly forecast the diurnal cycle also impacted substantially on the character and evolution of forecast spread. The persistent mesoscale features were represented reasonably well, however the detailed structure of these features had a fair amount of uncertainty.

THIS PAGE INTENTIONALLY LEFT BLANK

TABLE OF CONTENTS

LIST OF TABLES

THIS PAGE INTENTIONALLY LEFT BLANK

LIST OF FIGURES

THIS PAGE INTENTIONALLY LEFT BLANK

ACKNOWLEDGEMENTS

I would like to thank everyone who contributed to help accomplish this work. Dr. Wendell Nuss' extensive knowledge of mesoscale meteorology, guidance and patience during this whole process will always be appreciated. He helped me learn a great deal about the subject and was an invaluable part of this project. LCDR Dave Brown, thank you for your time, input and assistance, it is very much appreciated. I would also like to thank Dr. Doug Miller; without his model runs this project would not have been possible. I am also thankful for his assistance and expertise. Also, thanks to Bob Creasey for his willingness to help in moving my data, to allow for more disk space, for sharing helpful hints to cure writers block and for his general interest in what I was doing. Thank you to my classmates for the friendships and humor through these trying times of thesis completion.

Scott, thank you for all the help with the simplifying of my data processing. I do not know what I would have done with out it; it was above and beyond anything I ever expected. Thank you as well for your love and support during this venture.

I especially want to thank my Mom for all her encouragement; from dealing with me while working on this endeavor, to taking care of life's little things so I could focus on my work. Also, thanks for the proof reads, even though you don't fully understand the material!

THIS PAGE INTENTIONALLY LEFT BLANK

I. INTRODUCTION

A. MOTIVATION

Mesoscale models provide the user with a more realistic view of the atmosphere, capturing details of mesoscale phenomena with higher resolution (Doyle 1997 and others). However, this does not necessarily lead to an improvement in forecast skill because they are attempting to model things whose behaviors and time scales are not fully understood or observed. In order to have an overall increase in forecast skill, the model error for all variables must be reduced everywhere. A study by Weygandt and Seaman (1994) shows an increase in model error when just horizontal resolution is increased. The skill of many parameters decreased suggesting that other factors, such as model physics, vertical resolution, and initial conditions become more important as grid resolution is enhanced.

The impact of higher model resolution on other parameters is important because it impacts the skill of the model forecast. Consequently, there becomes a greater need to know about predictability on small scales.

B. PREDICTABILITY

Anthes and Baumhefner (1984) define predictability as the upper limit to forecast skill. He suggests that an inherent limit to the predictability of atmospheric motions exists because one cannot completely and accurately observe the atmosphere at all times and on all scales of motion. As a result, all forecast skill and predictability would eventually be lost given enough time, due to these inherent uncertainties in the initial conditions.

Lorenz (1982), another leader in predictability studies, describes the bounds of predictability. He considered the lower bound to be the skill of current forecast procedures, while the upper bound is based on the predictability of instantaneous weather patterns, or as Lorenz states, the predictability of the instability of the atmosphere with small amplitude perturbations. Lorenz (1982) suggests that the lack of predictability in the behavior of the atmosphere is evidence for this instability. He goes on to define a predictability time limit. This is the amount of time between the best estimate of the atmosphere based on observations and an estimate of its state at a future time, to the point at which the forecast looses all skill. After a forecast reaches this limit it is unusable, and basically is no better than guessing (Lorenz 1982). This predictability limit is strongly dependant upon the accuracy of the measure of the initial conditions.

Figure 1 is a graphical depiction of theoretical error growth. It compares the error associated with climatology, persistence and the numerical model output. The error in the numerical model starts small and then grows rapidly from the initial time step and is associated with model spin up. As the dynamic imbalances are resolved the error begins to decrease. There is a period of low error from which error begins to grow again due to the incompleteness of model physics. Finally reaching a point where the forecast no longer has skill.

Anthes (1986) also demonstrates the growth of error by using the variance of 500mb heights (Figure 2). He

compares the error associated with a forecast of climatology (E_c), a persistence forecast (E_{obs}), a model forecast (E) as seen in the previous forecast. He also shows the predictability error growth (E_p), which represents an estimate of the maximum obtainable forecast skill.

Lorenz first studied synoptic scale predictability in 1965. The result of his study demonstrated that the error growth rate was dependent upon the synoptic situation and that a 7-day forecast could be possible, but a month long forecast was out of the question (Lorenz 1965). The result of a later study, by Lorenz in 1969, included some small scale effects. This study indicated that if the large scale was observed perfectly, the small scale uncertainties would induce error on the large scale and grow as if errors existed in the large scale initially (Lorenz 1969).

The results of other early predictability studies suggest that predictability would decrease as the horizontal scales became smaller. The effect of synoptic pattern and weak versus strong instability was also found to alter the predictability. In summary, predictability had been found to vary with horizontal scale, season, geographic location, and synoptic pattern (Anthes 1986). It was also shown that when the same set of observations were added to different models they each had different error growths.

Anthes (1986) confirmed the results of Lorenz's 1969 study also indicating that the mesoscale was less predictable than the synoptic scale. Anthes also suggests that the uncertainty of one scale of motion would contaminate all scales due to the nonlinearity of the

atmosphere. Due to the energy exchanged among all scales of motion and the nonlinear nature of the atmosphere, the mesoscale reaches its predictability limit before the larger scales. Tennekes (1978) suggested that this nonlinear energy transfer was a result of 2 and 3-dimensional turbulence, implying that error on one scale would contaminate the other scales (Anthes 1984). Kuypers (2000) found while there was no correlation between synoptic and mesoscale error, the majority of the error at the smaller scales was dominated by the error from the larger scales.

Anthes (1986) describes the predictability error growth or representing the growth of initial small differences in a perfect model. He proposes that the reason different scales of motion were forecast with different skill levels is due to an inherent difference in the predictability error growth for each scale of motion. This also suggests that model error could grow faster than predictability error, resulting in forecast skill less than what predictability theory suggests. The estimate of this model error would be indicative of the possible improvements, which could still be realized. Contributions to model error would be from parameterizations, numerics, boundary conditions and initial conditions (Anthes 1986).

There is a general impression that mesoscale forecasts near topography are more predictable (Mass et all 2002 and others). The idea is that with higher resolution the presence of terrain is better represented helping to reduce the error and therefore increase predictability. Higher

resolution models better simulate the topography and therefore capture more of the topographically forced features. A study done by Weygandt and Seaman (1994) showed a decrease of mean error for topographically forced features, confirming that terrain increases predictability. The benefits to increasing model resolution for capturing topographically induced circulations were also seen in a study by Mass et al (2002).

The other half of this argument suggests that the presence of topography makes the mesoscale less predictable through an increase in error. It was found that the largest wind speed errors in the mesoscale were near the topography during the case of a landfalling front (Nuss and Miller 2001). It will also be shown in this thesis that the largest model errors are associated with regions of topography. The differences between model topography and reality can at times be significant, contributing to error.

C. OBJECTIVES

A suggested approach for examining the predictability of a mesoscale model is to determine the spread between the forecasts. The idea being that low spread events will be more predictable than those with high spread. It has been observed that if the spread is small, the skill of the forecast tends to be higher (Steenburgh 2002).

Since the spread is indicative of uncertainty it is used in this study to examine error growth and distribution. The spread was determined using the difference between the various model forecasts and model analyses. The amount of spread, or uncertainty, and the period and location of which it occurred are used to

characterize the predictability of the mesoscale wind field.

The Mesoscale Model version 5 (MM5), run in real-time by the Naval Postgraduate School (NPS), is used to construct lagged forecast wind fields in order to investigate mesoscale predictability based on a mesoscale model. The error growth for each forecast cycle was examined for the California summer, which extended from 01 May 2002 until 04 October 2002 and related to predictability theory.

II. MESOSCALE MODEL AND METHODS

A. MODEL DESCRIPTION

The Mesoscale Model version 5 (MM5) is used for all model runs and analyses for this thesis. Researchers at Penn State University and the National Center for Atmospheric Research developed and continue to support the MM5 (PSU/NCAR 2003). It is a limited-area, nonhydrostatic, terrain-following, sigma-coordinate model designed to simulate or predict mesoscale and regional-scale atmospheric circulations. MM5 can be run on a Unix machine or a Linux based PC. The computer power needed to run this model increases as mesh size and grid resolution increase (PSU/NCAR 2003). Dr. Doug Miller at NPS ran the MM5 used for this thesis.

The version used in this study is MM5V2.12, the second version of the MM5. This version of the model can be run hydrostatically or non-hydrostatically depending on what the user chooses. The basis of a hydrostatic model is the assumption of hydrostatic equilibrium. These models are better for global and synoptic features, since they do not account for much of the necessary physics necessary to model smaller features. Non-hydrostatic models basically define a reference state and the perturbations from that state. These models are preferred for mesoscale modeling because they account for vertical motions and accelerations rather than inferring them from the horizontal convergence and divergence, i.e. continuity. It becomes important to use a non-hydrostatic model when you begin to talk about

features that are similar in height and length scales and on the order of about 10 km.

As with all mesoscale models, MM5 requires an initial condition and lateral boundary condition for a model run, it is therefore coupled with a global model or another regional model. It uses the other model's output as a first guess for objective analysis or as the lateral boundary conditions (PSU/NCAR 2003). In this case, the National Centers for Environmental Prediction (NCEP) Aviation model (AVN) is the parent model providing the boundary conditions in the MM5 36-hour (h) forecast as well as the analyses and forecasts for the basis of the MM5 12-h forecast in the case of a cold start (Miller 2002).

A model cold start creates the analysis using climatology, or a prior analysis if available, and observations that have been assimilated into the model. The difference for a mesoscale model is that the synoptic forecast is interpolated down to the mesoscale and used with observations. This MM5 cold start is generated from the AVN analyses and forecasts, as AVN is the parent synoptic model. There were a very small number of cold starts over the data collection period; the majority were warm starts. A warm start combines observations with the model's most recent forecast, or first guess, in order to generate the next forecast. The observations are used to nudge the model towards reality. The MM5 in this study uses the 12-h forecast as the first guess for the 36-h forecast. Both types of starts can induce errors; it depends on the quality of the parent field and data assimilation.

MM5's vertical and horizontal resolution and domain size are variable, allowing the user to define them to their specific needs (PSU/NCAR 2003). MM5 defines its vertical, or sigma, levels in terms of pressure. The near ground sigma surfaces closely simulate the terrain in the MM5, while at higher-levels they tend to approximate isobaric surfaces (PSU/NCAR 2003). The advantage to using sigma over constant pressure or height surfaces is the fact that the sigma surfaces do not intersect the topography as the other surfaces do. This allows the user to easily increase the vertical resolution near the surface, enhancing the representation in the planetary boundary layer if desired. The number of sigma levels in the MM5 used here is 30 for all grids. Thirteen of these vertical levels are used to describe the portion of the atmosphere between the surface and 700mb.

The MM5 used in this study is a triple-nested model and therefore has three horizontal grid resolutions. The largest or the coarse resolution is 108 km (59 x 59 grid points); next is the fine resolution grid at 36 km (49 x 61 grid points); and the superfine grid at 12 km (91 x 127 grid points) is the smallest. These grids are nested over the west coast of the United States and California as seen in Figure 3.

B. VISUAL AND GEMPAK

VISUAL is a FORTRAN-coded diagnostic and display program that uses NCAR graphics utility routines to look at meteorological information (Nuss and Drake 1995). This program was used to examine the statistical data set at various pressure levels as well as vertical cross sections.

VISUAL also allows for generated plots to be printed for publication.

The General Meteorological Package, or GEMPAK, is a suite of application programs for the analysis, display, and diagnosis of meteorological data (UCAR 1998).

C. PROCEDURE

MM5 raw forecast data, in the form of GEMPAK files, were collected beginning 01 May 2002 through 04 October 2002, basically encompassing the California dry season. Each model run went out to a 36-h forecast, in 3-h increments. In order to ensure a three member ensemble, lagged forecasts were used. Lagged forecasting used the 24-h, 12-h and initial forecasts, which were all valid for the same time period, based on the assumption that there would not be a large difference between them. In a relatively unchanging synoptic regime, such as the California summer, this was a valid assumption. Due to the use of lagged forecasts, only the periods up to the 12-h forecast could be used. Only one or two members would be present in the ensemble if we had tried to use forecasts beyond the 12-h forecast. Statistics were calculated during the data processing. The mean wind speed and spread (difference in wind speed from the forecasts and associated analysis) were calculated. The spread becomes important because we believe this is indicative of model error.

The GEMPAK files were first interpolated from the 108km and 36km domains onto the 12km domain. No artificial effects resulted from the interpolation. This step of processing the data also allowed for it to be further

processed for statistics and plotted using the VISUAL program.

Next was an attempt to get a basic plan of how to categorize the synoptic regimes to create smaller groups. The data was plotted in VISUAL using 500mb heights and 850mb winds for each day at 0000UTC and 1200UTC (hereafter 00z and 12z model analysis). It was determined to divide the season into four categories based on the 850mb wind pattern to investigate the impact of different synoptic flow patterns. The four categories were: along coast flow (coast parallel), onshore flow, offshore flow, and weak flow. The flow over the region from Cape Mendocino to Big Sur was used to determine the analysis category. The data set was also examined as one large group.

Each day was then processed to determine the mean and spread of the wind field over the 12 km domain. The mean was the mean wind speed and the spread was the maximum difference in the wind speed between the three lagged forecasts. The program took three 12-h forecast periods with five forecasts for each period (3 hour forecast intervals). Table 1 is an example of how the lagged forecasts were analyzed. In this example the program used the 24-h forecast from the 00z analysis, the 12-h forecast from the 12z analysis on the 30th and the 00z analysis on the 1st. The program used those times and then went out to the next forecast, in three-hour intervals.

Step 1	30/00z f24	30/12z f12	01/00z f00
Step 2	f27	f15	f03
Step 3	f30	f18	f06
Step 4	f33	f21	f09
Step 5	f36	f24	f12

Table 1: Example of how the statistical analysis program, calc-stats, processed the forecast data. In the form of: 30/00z f24 = 30(day)/ 00z (model analysis) f24 (24 hour forecast).

The next step was to average all of the mean data and all of the spread data for each time period and forecast. This was done for each flow pattern (along, onshore, offshore and weak) as well as for the entire data set. An input file, which consisted of each date and analysis time, was first created for the flow patterns and then processed for the average. These data sets were not broken down by model start time, so 00z and 12z were averaged together. In order to create a manageable input file for the whole season each month was averaged by analysis time (i.e. each month had two files a 00z and a 12z). The months were then averaged together into larger input files representing the 00z and 12z for the summer season. The processing was done in this manner due to the amount of data files and does not affect the results since it is a simple averaging of data.

This data was further analyzed with plots created in VISUAL. The levels 850mb and 500mb were plotted to describe the synoptic patterns over the entire domain at those levels. All of the plots created were from the statistical data, the mean wind speed and its spread. The

plots created were for the seasonal data as well as the four flow categories. Four West-East cross sections were chosen as illustrated in Figure 4. The cross sections were chosen for their differences in terrain. The vertical cross sections were plotted for each model start time, 00z and 12z, as well as for the 00 to 12 hour forecast of each run (forecasts are every 3 hours). The vertical cross sections for the four flow patterns were also plotted by forecast time. Since these forecast times were averaged together in the previous step they contain both 00z and 12z model start times and therefore have only one set of forecasts (not two like the summer case). Horizontal plots were also created in a similar fashion for each of the data sets.

The final step used to analyze the data sets was to construct an average of the spread over the entire domain for each sigma level. The output of this program was by level, from the surface to 500mb (21 levels), and the mean value of the spread field for each forecast (to 12 hours) of the 00z and 12z model start times. This program was initially run using the entire 12 km domain. However, we found this to be strongly influenced by the large area over the ocean, where the spread decreased through the 12-h period independent of the synoptic situation. These level averages were not representative of the regions near topography where the spread changed significantly with each forecast as seen in the VISUAL plots. The increased spread near the topography was essentially masked by the low spread values over the water in the average. In an attempt to better illustrate the over land performance, the averaging domain was reduced to limit the amount of data

over the water and focus on the coastal and inland topographical effects. This new domain considered the eastern two-thirds of the 12 km domain and was therefore no longer dominated by the trends over the ocean.

III. GENERAL DISCUSSION

A. SUMMER CLIMATOLOGY

The climate of California is quite varied; along the coast it is mild and tends to be cooler in the northern and central parts of the state, while the southeastern region is hot and dry. California's summer season, also the dry season, begins in the late spring and continues until October when the wet season begins. The primary synoptic feature during this time period is the East Pacific (EASTPAC) High. This dominates the region with large-scale subsidence and produces northwesterly surface winds over the eastern Pacific Ocean. These northwesterlies drive the Ekman transport along the west coast of North America forcing the surface waters offshore. This allows the cold deep water to rise to the surface resulting in very cool ocean temperatures near the coast. The strong subsidence and cool ocean temperatures result in a strong low-level inversion and a well developed boundary layer through out the region.

A thermally induced surface low over the desert Southwest and the interior region of California is also present during the summer months as a result of significant daytime heating. This thermal trough helps establish a strong cross-coast pressure gradient and strong northwesterly flow.

B. OVERVIEW OF DYNAMICS

There are several mesoscale events that occur during the summer season. The prominent features were seen in the

analysis of this thesis. This section describes the basic dynamics of these features.

1. Coastal Jet

The California coastal jet is present a majority of days during the summer months. The jet flows along the coast towards the south with the strongest winds near the coast and weaker winds offshore. Its maximum is neither at the surface nor up against the coastal mountains, but rather slightly elevated and away from the coastal terrain (where the maximum pressure and temperature gradients are located). This is due to surface friction, which retards the wind closer to the surface. The jet is initiated by the cross-coast pressure gradient established by the synoptic regime and is forced by the coastal topography. Wind speeds in the jet core can be greater than 40 knots with little diurnal variation.

There is a strong baroclinic structure at the coast and a well-mixed marine boundary layer offshore. The depth of the inversion increases offshore due to the weakening of the synoptic subsidence and the warmer sea surface temperatures. The isentropes slope with the inversion leading to the coastal baroclinic structure and, through thermal wind relation, leads to a low-level wind maximum. It has been observed that the stronger the isobaric slope the stronger the jet can become (Nuss 2002).

Coastal topography also plays a role in jet dynamics. The northwesterly flow is typically blocked by the terrain due to the presence of a strong low-level inversion and is turned down gradient parallel to the coast. The flow is strongest near the coast and weakens offshore as it

approaches the Rossby radius of the mountains. This will occur even if there is no slope to the inversion. This is also consistent with the structure implied by the thermal gradient (Nuss 2002).

2. Mountain and Valley Breezes

The mountain and valley winds are diurnally forced. They are generally favored when there is weak synoptic flow and a weak pressure gradient. Formation of these breezes depends upon the contrast in surface temperatures, the difference between daytime heating and nighttime cooling, the orientation of the mountain slope (heating is strongest on the southern and eastern facing slopes), and the direction of the synoptic flow. It is also important to have mostly clear skies in order for the strongest heating and cooling to occur. (COMET 2003)

a. Mountain Breeze

The mountain breeze consists of an up-slope and down-slope wind. When the sun rises it begins to heat the slopes of the mountain and the air above causing the warmer air to rise up the slope. The result of this up-slope wind is subsidence in the valley. By the afternoon the up-slope winds are at their peak. As the solar heating decreases and radiative cooling begins the winds near the surface begin to reverse while those higher in the boundary layer still remain up-slope winds. As the mountains cool the whole system reverses due to the development of cooler, denser air. This action results in the down-slope winds. The air in the valley rises in response to the down-slope winds (Ahrens 1994).

b. Valley Breeze

The valley breeze occurs along with the mountain breeze. The up-slope winds begin shortly after sunrise and after sufficient heating has occurred in the valley. Later in the morning the winds become up-valley winds. The wider and deeper the valley, the longer it takes for the winds to shift direction. The up-valley breeze lasts until after sunset. Once adequate cooling has taken place the down-valley breeze takes over. This lasts until after sunrise when the cycle begins again. The valley breezes occupy the lower 10 to 30% of the total valley depth. The average up/down-valley breeze speed is 10 m/s, but can be stronger depending on the strength and depth of the inversion. These winds tend to accelerate as they travel through the valley. As they exit the valley they gradually slow as the flow spreads out (COMET 2003).

3. Thermal Effects

Thermal circulations are very similar to sea breeze circulations, but involve the difference of heating over land instead of the land and water temperature differences. If there is no variation in temperature (or pressure) in the horizontal over the land there will not be a circulation. In this situation isobaric surfaces are flat. When the atmosphere is heated in one area more than another, or cooled more in one area versus another, the isobaric surfaces become sloped. They are close together over the cooler region and spread apart over the warmer region. This slope leads to a pressure gradient aloft, with the air moving from high to low pressure. There is an associated vertical circulation with the horizontal one,

caused by warm air rising and cold air sinking. The surface lows and highs created through this process are referred to as thermal highs and lows.

4. Mountain Waves

Mountain waves are created when the wind blows over a ridge; the air parcels are displaced vertically and, if the air is stably stratified, will descend and may oscillate about their equilibrium level. The result is a gravity wave, referred to as a mountain or lee wave. For ranges that are less than 100 km in width the perturbations seen in the wind fields are primarily in the vertical, where as ranges with widths greater than 100 km the perturbations are predominately in the horizontal (Durran 1986).

The initial perturbation of the air parcels triggered by the mountains was seen most predominately in the Central California cross-section due to interaction with the Sierra-Nevada Mountains. This range in eastern California is about 690 km (430 miles) long and 60–110 km (40-70 miles) wide, with many of its peaks reaching 4270 m (14,000 ft) or higher. The perturbation of the air parcels in this case is in the vertical due to the width of the range.

The stability of the atmosphere plays a role in the formation and appearance of the mountain waves. These waves are buoyancy driven oscillations and therefore need a stably stratified environment in order to support propagation. If a weaker, stable layer is above a stronger, stable layer the wave amplitude will decay with height. The waves could also be trapped in this case. The period of these oscillations, or the Brunt-Vaisala frequency (N^2), and the frequency imposed by the terrain as

the air flows over are also important in determining the vertical propagation, the amplitude, and trapping of these waves.

IV. RESULTS

A. OVERVIEW OF RESULTS

The structure and characteristics of mesoscale uncertainty are illustrated in four cross sections taken through the 12 km domain (Figure 4). The northern most cross section proceeds through Cape Mendocino and the northern parts of the Sierra-Nevada mountain range; the next cross section goes through San Francisco and the central region of the Sierra-Nevada range; the third cross section runs near Point Conception toward Lake Havasu; and the final, most southern cross section extends through San Clemente Island, just north of San Diego into Arizona. Each cross section was chosen due to the differences in topography. All cross sections start offshore, in order to capture the majority of the coastal jet feature, and end just east of the California border. The persistent mesoscale features seen in this study will be examined further. These features include the coastal jet, mountain and valley circulations, topographic effects, and the structure of the model atmosphere with height.

The expected trend of error in wind speed to grow over time is not observed in this study (Figure 1). Although the spread did increase between the analysis and the 3-h forecast of each forecast cycle, the spread did not significantly decrease and then slowly increase as might be expected as the model adjusts to the initial conditions. Instead, the spread of the wind speed tended to remain rather large through the 12-h forecast cycle as observed in the level-average tables, (Tables 2-7). This is

particularly true at lower levels, while in all cases the spread increased in the upper levels throughout the 12-h forecast cycle. There is also a difference in the 00z and 12z forecast cycles. The 00z cycle has significantly more spread through the 12-h forecast than the 12z cycle does, at all levels.

A diurnal cycle is also observed in the model. The 00z forecast series have more uncertainty associated with all of the features than the 12z cycle does. This is seen in all of the forecast hours. There is an increase in uncertainty in the 3-h forecast for both, however the 00z forecast cycle continues to have large spread values through the remaining part of the forecast. The 12z forecast cycle does not continue to have large spread values after the 3-h forecast.

The primary relationship between spread and mean wind speed found in this study is that as mean wind speed increases, the spread also increases. This is seen in all cross sections, as an increase in spread with height, and is associated with the larger mean wind speeds due to the stronger dynamics aloft. In addition, the mesoscale features with higher wind speeds, such as the coastal jet, also have higher spread as observed in the cross sections.

B. COASTAL JET

The mean wind fields in MM5 clearly depict the coastal jet throughout the summer season (Figures 5-27). The jet extends from Northern California where it is most prevalent, to Southern California. Using spread as an indicator of uncertainty, the intensity and position of the jet core exhibited considerable variation. The mean jet

tended to be lower in the atmosphere and further to the west than the position of the spread maximum. In addition, the spread was larger at higher mean wind speeds.

The cross sections demonstrate the vertical structure of the coastal jet. The strongest winds are closest to the coast and weaken offshore. Although the jet typically slopes up with the inversion from the coast as it moves offshore this slope is barely evident in the cross sections represented in Figures 5 and 6. The solid lines in these figures represent the total mean wind speed, and the dashed lines represent the spread. This convention is used throughout the rest of the vertical cross sections and horizontal plots. The coastal jet has little diurnal variation; a comparison of Figures 5 and 6 show a slightly stronger jet at 00z f03 than at the 12z f03 forecast. Figures 5 and 6 show that the jet core is strongest just after the maximum heating and is weaker and further from the coast during the cool part of the diurnal cycle. The spread however, remains close to the coast during these periods. In fact, the position of the spread maxima for all of the cross sections and times remained close to the coast. It did not change position with the slight movement of the jet core.

The magnitude of the jet is the strongest in the northern most cross section, which has a range of mean wind speed values of 11-13m/s and spread values of 3.5-4.0m/s. The central cross section was slightly lower with mean wind speed values of 10-12m/s and 3.0-4.0m/s for the spread. As expected, the numbers continued to decrease as one moved further south, since the coastal jet tends to weaken

towards the south. The values at the Point Conception cross section were 9-10m/s for the mean wind speed and 2.5-3.5m/s for the spread. The weakest of all is the Southern California cross section. It has a range of mean wind speed values of 8-9m/s, with the spread having a range of 2.5-3.5m/s.

Examining the time variation of the jet structure and uncertainty reveals that the coastal jet is stronger in the 00z forecast cycle than in the 12z cycle. The 00z forecast cycle in the Northern cross section is strongest at the 3-h forecast with a mean wind speed of 13 m/s and spread of 4.5m/s (Figure 5), while the 12z is at its weakest at the 6-hour forecast with a mean wind speed of 11 m/s and spread of 3.5m/s. A reason for this is the 00z run begins at the warmest part of the day, 4pm local time. The jet is well represented in the observations that are assimilated into the model for that run. The jet in the 00z forecast cycle increases at the 3-h forecast from 12m/s to 13m/s with a spread increase of 0.5m/s, from 4.0 to 4.5 m/s. The coastal jet weakens after the 00z f03 forecast for the remainder of the forecast period. The only exception is the 12-h forecast in the Point Conception cross-section where there is an increase in jet speed and spread.

This pattern of jet intensity and spread for the 00z and 12z forecast cycles varied to some extent with location. The magnitude of jet speed and spread for the 3-h forecast of the 00z forecast cycle, is not the strongest in all of the cross sections. The cross section near Point Conception has its strongest 00z jet at the 3-h forecast. The other cross sections have their maxima at the 6-h

forecast for the 00z series. The weakest jet speed in the 12z run is consistently the 6-h forecast, with the exception of the Southern California cross section where the weakest is at the initial time.

The 850mb horizontal plots show the varying horizontal structure of the coastal jet in the different synoptic flow regimes as well as the small changes in the summer case as a result of diurnal effects. These plots are not ideal, in that they do not go through the maximum of the coastal jet, but instead pass right above it. However, the 850mb winds can affect the intensity of the coastal jet and are generally indicative of its horizontal location (Nuss 2002).

The 00z and 12z forecasts show that the coastal jet is strongest in Northern California, weakens around the Central Coast and continues to weaken as one looks south (Figure 7). The along coast flow shows the coastal jet extending strongly into the Southern California region, as noted by the increased wind speeds along the coast (Figure 8). In all of the other flow cases the coastal jet begins to relax further to the north. The offshore flow, Figure 9, is very similar to the 00z and 12z jet. The jet is slightly stronger offshore (8 vs. 10m/s) as it extends down the coast along 115W, but is still weaker in Southern California. The onshore flow does not have a strong jet with mean winds less than 5m/s even in the northern part of the state (Figure 10). A weak increase in mean wind speed as one moves offshore is apparent and the only indication of a coastal jet. The maximum mean wind speed of the jet at this level is 7m/s, where the previous cases were 9m/s

or greater. The weak flow has a very prominent jet in Northern California, with mean wind speeds over 8m/s, but the flow rapidly weakens to less than 3m/s just north of San Francisco Bay (Figure 11). The weak flow case has this weakening of the flow along the coast further north than any other case.

Variations in the coastal jet and its associated spread under the four different synoptic flows are also evident in the cross sections. For example, in the along coast case, the coastal jet is stronger in Southern California than in any other flow regime (Figure 12). The spread in this region is no larger than in the summer average, despite the increase in mean wind speeds. The location of the spread also remains near the coast. The constant spread values for the along coast flow regime compared to the summer average, suggest that MM5 is less sensitive to synoptic variability in this flow regime.

The weak flow coastal jet had very large spread values. It demonstrates large uncertainty, which is seen in the spread as mean wind speed increases. It also shows the inability of the model to forecast the position and intensity in a weak flow situation. In this flow regime, the Southern California region had the weakest jet. The uncertainty here is more from variation in intensity than in position, since the spread contours match up relatively well with those of the mean wind speed (Figure 13).

The along coast flow cases do not have the strongest coastal jet in all cross sections as might be expected. The Cape Mendocino section has a mean wind speed value of 13m/s for all forecast times with spread values ranging

from 2.5m/s to 3.25m/s. Nevertheless, these values are not the largest. The weak flow Cape Mendocino case is the strongest and also has the largest uncertainty associated with it. It has a constant mean wind speed of 14m/s over all forecast periods and a spread ranging from 4.5m/s to 5m/s. The offshore flow Cape Mendocino case is also larger than the along coast, with a mean wind speed of 14m/s for all forecast times and a spread of 3.0-3.25m/s.

C. MOUNTAIN AND VALLEY CIRCULATIONS

Mountain and valley breezes are seen in all of the cross sections to varying degrees. The northern cross sections have both, as does the Point Conception profile, while the Southern California cross section has a mountain breeze.

In the northern most cross section, a valley breeze is noticed between the coastal mountains and the Sierra-Nevadas. This feature exhibits a lot of variability (Figure 5). During the 00z forecast cycle the mean wind speed of this breeze is between 5 and 8m/s, with the strongest times at the 00z f03 and 00z f06 forecasts. The spread throughout the 00z forecasts varies as well. The range was 3.0-4.5m/s, yet the largest spread does not always correspond to the larger mean wind speeds here as observed in other features. The large spread associated with this feature most likely occurs during the transition from an up-valley to a down-valley breeze. This switch transpires after diurnal heating and cooling begins. The 12z cycle starts off with a mean wind speed of 6m/s and a spread of 3.5m/s, as the forecast time increases the mean and spread of the wind field decreased to 4m/s and 2.5m/s,

respectively. MM5 has difficulties with the cooling part of the diurnal cycle, which adds to the uncertainty in the forecast skill of this feature. This breeze is one of the weaker features, with low mean wind speeds, but the associated spread is large. The greatest spread also occurs at the time when the model is staying warm instead of cooling in the 00z forecast cycle. These same characteristics are observed for all of the different synoptic flow cases as well.

The 12z f03 forecast of the San Francisco Bay cross section shows increased uncertainty in the region near the steep slope of the topography, which is associated with a mountain breeze (Figure 14). This feature is not very strong, but is highly variable. Through the rest of the 12z forecast the feature is weak but predictable since the uncertainty is very low. Unlike the coastal range, which has a high amount of uncertainty throughout both forecast periods, the increased spread is only on the windward side at the one forecast time. MM5 may not be fully resolving the steepness of the windward slope in this region. This uncertainty is present during a forecast from the cool part of the cycle (12z f03), which MM5 handles well. MM5 may over heat this western facing slope too early causing a difference in the transition from down-slope to up-slope winds as well as in mean wind speed.

This mountain breeze is also seen in all of the cases for the different synoptic flows. As with the summer 12z case (Figure 14), all of the flows similarly show a spread maximum at the 3-h forecast that decreases significantly in the later forecasts. All of the cases have mean wind

speeds of 4m/s in that region. The weak and offshore flows have a spread of 3.5m/s, which is greater than the 3.0m/s spread of the along coast and onshore flows.

The lee side of the coastal mountains in the Southern California cross section has a region of high spread in all forecasts of the summer case and in all of the various synoptic flow cases (Figure 15). The largest spread is in the initial and 3-h forecasts for all cases. There is a trend for the maximum spread to weaken beginning with the 6-h forecast in all cases as well. This area of large uncertainty is probably due to the model not correctly portraying the mountain breeze.

D. TOPOGRAPHIC EFFECTS

The characteristics in the four different synoptic flow cases are surprisingly similar to each other and to the summer average. This is not expected since the regimes are all very different; along coast, offshore, onshore and weak flow. It was anticipated that the mesoscale features noted would be different for each flow pattern due to their potential differences in interaction with topography.

The large region of high spread seen on all of the Southern California cross sections on the lee side of the coastal range is a result of MM5 incorrectly forecasting a mountain breeze (Figure 15). This feature is present at all time steps and cases suggesting that MM5 over forecasts the up and down-slope winds in this region. The mean winds are rather light throughout the season, but the spread here is exceptionally high, especially during the 00z forecasts, when the model should have been cooling the atmosphere. The uncertainty during the warming cycle is large here as

well, but less than during the cooling cycle (>5m/s vs. 3.5m/s). The model's diurnal problem most likely adds to the uncertainty seen in the 00z run. Another possible explanation for this large spread is that MM5 is not showing the across mountain flow properly. This flow is due to the cool temperatures over the water and the warm temperatures over land to the east of this range. It is also possible that the model is not correctly forecasting the low level stratification allowing a mountain breeze to take place when in fact it is being prevented by the stratification.

The fluctuations seen in the wind fields over the mountains are presumably due to flow interaction with the topography and could be representative of mountain wave formation in the model (Figure 16). Durran (1986) showed that for steeper slopes the wave amplitude is larger, as is the tendency for vertical propagation. This is seen in the different cross sections as well. In general the spread in the upper levels is higher, but in the regions of these waves the local spread is no larger than the environment. The spread fields are perturbed as well, so in fact, the spread over the mountains is actually lower than the spread of the surrounding atmosphere at a given level.

In the central cross section (Figure 16) the terrain has an effect on the mean wind field that extends above 500mb. This cross section is the only one with significant topography; the eastern portion is where it crosses the Sierra-Nevada Mountains. The mountains cause a perturbation in the mean and the spread over the peak. This perturbation is a result of the air flowing over the

mountains and probably the mark of mountain wave formation. The northern and southern cross sections also show perturbations in the spread and mean wind fields, though not to the extent of the central section. The effect of the coastal topography in those sections reaches only to the 650mb level.

All of the four synoptic flow cases for the Central California cross section show perturbations in the mean wind field and spread above 500mb over the Sierra-Nevada Mountains as in the summer plots (Figure 16). Similar to the summer case, these waves are the response of the flow as it runs into the topography and are presumably an indicator of mountain wave formation. The along coast and onshore cases show the largest amplitude of these waves (Figure 17). The offshore case demonstrates smaller amplitude waves which decrease quickly with height (Figure 18). The weak flow case has the perturbations as well, but the amplitudes are not as great (not shown).

The offshore flow cross sections are very similar to the summer average cross sections as far as seeing perturbations associated with mountain wave formation. In all of these cross sections the perturbations stay below the 650mb level. This is true for the weak flow cross sections as well. The along coast case does as well, except for the Point Conception region where very small amplitude perturbations do occur near the 500mb level. The amplitudes of the waves decrease with height and the lower level disturbances do extend downstream (Figure 19). The weak flow Point Conception region is an exception since the waves in the mean wind and spread propagate above 500mb.

The mean flow in this region was the slowest with speeds between 4 and 6m/s.

The onshore flow case in the Southern California cross section shows perturbations from the coastal topography extending above 500mb (Figure 20). The amplitude of the perturbations decreases with height and continues downstream. This is different than all of the remaining Southern California cross sections where the perturbations due to topography remain below the 600mb level and may be due to the stronger cross mountain flow in this case.

E. DIURNAL VARIATION

The portion of the diurnal cycle sampled over the 12 hours impacts the evolution of uncertainty. In the 00z forecast cycle, the spread grows significantly until the 12-h forecast. Conversely, the spread in the 12z cycle does not increase as much until the 9 and 12-h forecasts (1pm and 4pm local time). 00z occurs at the maximum of heating for the day, 4pm local time. It is suggested that the model tries to keep the atmosphere warm longer, having difficulties with the cooling portion of the diurnal cycle. 12z is at the cool part of the diurnal cycle and the increase in spread at the 9 and 12-h forecasts demonstrates the ability of MM5 to better represent the warming portion of the diurnal cycle. This trend reveals the weakness of MM5 to cool the atmosphere in the 00z forecast cycle. The four synoptic flow cases are not separated by model run and therefore the diurnal effects are averaged together. These effects are not observed in this manner for those cases.

The Point Conception cross section illustrates this effect of model start time with respect to the diurnal

cycle (Figures 21 and 22). The terrain in this cross section is such that some surfaces begin to heat before others, which results in a thermal circulation. The 00z run shows that the model maintains a stronger circulation since it does not cool down very well. This is manifested by an increase in spread from the f00 to f06 forecasts. The 12z run handles the warming part of the diurnal cycle well. MM5 picked up on this circulation. The error is low and wind speeds are fairly strong. Once the cooling begins, the temperature gradient relaxes, the mean wind speeds decrease and the spread increases. The higher spread at this time is due not only to the slow cooling of the model but also due to the inherent lack of predictability of light and variable winds.

Diurnal effects do not considerably affect the coastal jet. However, MM5 showed that the jet is stronger during the warmer parts of the day. This suggests that the model is able to represent the cross-coast thermal gradient and the inversion relatively well. As noted in the earlier section on the coastal jet, the jet movement in towards the shore and away from it, as well as intensity differences, are due to the model representation of the diurnal cycle.

F. STRUCTURE WITH HEIGHT

The spread of the wind speed is found to increase with height, which is a result of the increase in wind speed with height due to stronger dynamics aloft. The average spread was 3.0m/s or greater at heights above 600mb in all cross sections. This was also seen on the level average tables for all (Tables 2-7).

In all of the vertical cross sections it is observed that as one moves up in the atmosphere, the spread increases. At the higher levels the synoptic scale should have more of an influence, implying that the winds at higher levels should be forecast with less uncertainty. Since the opposite is seen it suggests that the mesoscale 12km grid is responding to error growth from the synoptic scale. This is also supported by the fact that the 500mb spread is greatest at all forecast times and for all cases. The spread at 500mb also increases as forecast time increases, which is consistent with synoptic scale error growth. The synoptic scale should dominate at the longer forecast times, especially at the higher levels. This is also seen in the level average tables. These trends will most likely increase if the forecasts are run for longer periods of time.

Scale interaction is noted in the spread values in the plots and in the level averages (Tables 2-7). There is evidence of large spread in the upper levels suggesting that the synoptic scale error is beginning to affect the model level by level. The growth is seen in level 21 (500mb) and propagates down with increasing time. This trend will probably continue out past the 12-h forecast, if this study were able to do so.

In the lower levels spread decreases after the initial forecast period increase, yet had we been able to see longer forecasts we probably would have observed an increase at these levels, as the synoptic scale error would begin to dominate the forecast. At the same time the error

from the surface infiltrates the levels above it and can be seen slowly increasing with forecast time.

The 500mb plots show no interaction with topography, though the perturbations due to the vertically propagating waves over the Sierra-Nevada range could be seen in some plots (Figure 23). The mean wind speeds and spread were largest in these plots. The 00z forecast cycle continues to increase in spread throughout the 12-h period. The 12z increases for the first two forecasts, decreases at 12z f06 and 12z f09 finally increasing at the last forecast. As expected, there is no evidence of a coastal jet in any of the 500mb plots. The mean winds in the flow cases do show evidence of the direction of the synoptic forcing in each group (Figures 24-27). The along shore flow experienced the strongest forcing from the northwest, since this is where the strongest mean wind speeds are located (Figure 24). The offshore flow cases have the significantly stronger mean wind speeds to the north, as did the onshore flow case (Figure 25 and 26). However the onshore flow case has stronger mean wind speeds. The strongest mean wind speeds in the weak flow case occur in the northeastern region of the domain, suggesting this is where the dominant synoptic forcing is located (Figure 27).

The spread at the low levels, where the flow interacts with terrain, is much larger than it is at the higher levels. This is seen in all of the plots as definite features near the topography. The spread in those mesoscale regions frequently is larger than 2.5m/s. The spread at the upper levels is greater than 2.5m/s above 600mb over a broad region for all cases and forecast

periods. This large low level spread is not seen in the statistics (Tables 2-7). This is due to the averaging of the entire level. These large uncertainties are in such a small part of the domain that they basically get masked in the average by the other regions in the domain with low spread values. This indicates that low=level uncertainty is tied to mesoscale features, while upper=level uncertainty is more tied to synoptic scale features.

VI. DISCUSSION AND CONCLUSIONS

A. DISCUSSION

It was noted that a common characteristic of mesoscale models, the exaggeration of thermal circulations with topography, also exists in MM5. MM5 seems to force a mountain breeze even though it may not actually occur. This could be due to the fact that MM5 is having trouble accurately forecasting the low level stratification which would inhibit such a strong mountain breeze as illustrated in the Southern California cross sections. It is also possible that MM5 has difficulty with steep mountain slopes. Recall that MM5 is a terrain following model so it sees the winds on the slope of the mountain as horizontal winds. It then tries to force the circulation from the high-pressure valley to the low-pressure mountaintop despite the environmental characteristics, which may impede the actual formation of this breeze.

1. Topography

The thought that topography imparts greater predictability is not shown in this study. Whether it is the physical representation of the terrain in the model or the circulations that result from its presence, it is illustrated here that the largest source of uncertainty is the topography. Figure 28 depicts MM5's version of California's terrain.

The terrain in the model is a lot smoother than the real terrain. MM5 also sees mountains as steps rather than a steep slope. There are differences in the model topography as well. A barrier may or may not exist to the

extent that it does in reality, preventing flows from being represented correctly and increasing error. The studies that demonstrated improved skill due to topography may have had a better terrain representation or improved model physics.

The results of this study suggest that near and around the topography are where the lowest skill is and the greatest reduction of the predictability of this model. This result is also supported by the low and rather constant spread values over the Pacific Ocean. There is a higher level of predictability here than over land and less mesoscale structure in general. The valleys also had large changes in spread. MM5 may not be forecasting the valley breezes properly, which is also due to differences in the representation in terrain.

2. Diurnal Cycle

The results of this study show that the model does not accurately portray the diurnal cycle, and that is another large source of uncertainty. The observed patterns of error growth and decay support this. The 12z run follows the trend that one would expect and is reflected in Anthes' error curve (Figure 2). The spread growth in the 00z forecast cycle does not resemble the error curve in Figure 1 or Figure 2. The uncertainty seen here was in part due to the model's inability to fully capture the diurnal cycle. MM5 did not cool as fast as the atmosphere keeping the model warmer longer. This lead to large spread values through the forecast cycle.

B. CONCLUSIONS

Error growth is affected by many different variables. In this study we only explored the wind fields our attempt to provide insight into the predictability of a mesoscale model. On the whole, the basic characteristics of the summer season and the flow cases are very similar. This therefore suggests that the overall uncertainty of primary mesoscale features in this model is not that large. This is significant when trying to determine the predictability of features in a model. The consistency in capturing the dominant mesoscale features is encouraging, although the predictability of the detailed structure can be quite large

The standard error growth with respect to time, as seen in Figures 1 and 2, was not observed in this study. The initial uncertainties were largest in the first time step. Upon further examination of the level averages we saw that there is no one point in time that continually has the minimum spread values. The location of the minimum spread changes with location and case. This suggests that either no model adjustment to the initial conditions occurred or it occurred prior to the 3-h forecast. More likely is that the large spread at the analysis time masks any mesoscale error growth. This limits our ability to assess actual predictability error growth, but clearly highlights the uncertainty in mesoscale structure and the inability of the model to correct for this uncertainty.

C. SOURCES OF ERROR

There were sources of error in the way that we chose to approach this study. The lagged forecasts while indicative of synoptic scale variation were not able to

adequately represent small mesoscale perturbations with the 12-h time lag. A mesoscale ensemble with small mesoscale perturbations would be a better approach. However, the inability to consistently represent mesoscale details at the initial times in the model, found in this study, is problematic for any ensemble approach.

The region that was used to determine the flow categories left out Southern California. Hence, those cross sections were not always in a flow defined by the category they were placed in. This also affected the inland regions. The flow affecting the valley breeze could have been oriented in such a way as to result in position or intensity changes. These flows were not grouped together. The flows were also not indicative of the flow experienced by the inland mountains, such as the Sierra-Nevada range.

These errors could be removed by averaging multiple summer seasons and would potentially provide better insight to the predictability of this model.

D. FURTHER STUDY

In order to make this study complete, several other aspects should be considered which provide opportunities for further research. Several are listed here.

1. Research the Other Seasons

Other seasons need to be examined in order to see what happens during the transition seasons and in the winter. Other mesoscale features will arise; there will be more synoptic scale forcing events (summer was quite uneventful); and error trends will vary due to those

differences. Other weather patterns could provide different results.

2. Study Numerous Summer Seasons

Collect data over several summers. A more or less predictable feature could mark each summer skewing the results. Averaging these summers would lead to a better idea of error and predictability.

3. Research Different Model Parameters

It is also important to study parameters other than wind. This should be done for this data set as well as for other seasons. Model error growth and predictability patterns found here based on winds may not hold for all parameters.

4. Topography

Terrain played a large part in the error of this study, due to the model terrain being smoother than reality. Improving model topography would provide different, possibly more accurate, error results.

5. Compare with Observations

Observations should be compared to the data set to see if the features noted are still valid. The perturbations over the mountains in the wind field are present through out all the cases. Observations would show if this actually occurs as constantly as the model suggests.

6. Additional Statistical Techniques

It would also be useful to examine the data set using other statistics. This may shed more light on the subject providing different results. The very basics were used here, mean and spread, and still provided some useful results.

THIS PAGE INTENTIONALLY LEFT BLANK

APPENDIX A. TABLES

Level	Pressure (mb)	00z f00	00z f03	00z f06	00z f09	00z f12
1	22m AGL	2.214	2.002	1.994	1.942	1.908
2	1010	2.389	2.422	2.331	2.218	2.174
3	1000	2.544	2.637	2.522	2.375	2.314
4	990	2.623	2.854	2.734	2.558	2.478
5	980	2.672	3.000	2.911	2.700	2.599
6	970	2.672	3.060	3.001	2.778	2.654
7	960	2.639	3.063	3.027	2.806	2.665
8	950	2.614	3.061	3.041	2.825	2.671
9	925	2.615	2.962	2.962	2.784	2.645
10	900	2.496	2.881	2.889	2.724	2.614
11	875	2.473	2.839	2.862	2.706	2.611
12	850	2.523	2.863	2.913	2.748	2.651
13	825	2.480	2.899	2.994	2.856	2.731
14	800	2.523	2.916	3.015	2.905	2.773
15	775	2.570	2.885	2.978	2.877	2.772
16	750	2.609	2.859	2.948	2.863	2.781
17	700	2.777	2.916	2.973	2.946	2.905
18	650	2.947	3.089	3.128	3.140	3.136
19	600	3.242	3.341	3.365	3.371	3.397
20	550	3.480	3.570	3.582	3.632	3.697
21	500	3.728	3.765	3.837	3.959	4.047

Table 2. Level Average: Summer 00z
Average spread for the 12km domain at each level and forecast period.
AGL: Above Ground Level

Level	12z f00	12z f03	12z f06	12z f09	12z f12
1	2.406	2.152	1.878	1.773	1.802
2	2.424	2.292	2.147	2.020	1.989
3	2.632	2.452	2.230	2.097	2.070
4	2.729	2.606	2.297	2.169	2.167
5	2.870	2.715	2.324	2.193	2.225
6	2.962	2.772	2.325	2.178	2.232
7	2.988	2.801	2.311	2.134	2.202
8	3.006	2.813	2.305	2.099	2.175
9	3.013	2.801	2.327	2.068	2.134
10	2.895	2.793	2.363	2.087	2.127
11	2.875	2.799	2.394	2.126	2.144
12	2.942	2.796	2.393	2.154	2.177
13	2.943	2.810	2.445	2.223	2.246
14	2.932	2.810	2.527	2.310	2.320
15	2.879	2.798	2.604	2.394	2.380
16	2.828	2.803	2.678	2.477	2.439
17	2.919	2.885	2.817	2.655	2.605
18	3.017	3.023	2.983	2.895	2.889
19	3.201	3.246	3.217	3.169	3.187
20	3.436	3.484	3.475	3.411	3.443
21	3.720	3.736	3.713	3.649	3.693

Table 3. Level Average: Summer 12z.
Defined as in Table 2.

Level	f00	f03	f06	f09	f12
1	2.130	1.861	1.756	1.668	1.644
2	2.116	2.068	1.994	1.818	1.721
3	2.281	2.260	2.131	1.929	1.827
4	2.378	2.445	2.269	2.057	1.962
5	2.479	2.590	2.387	2.164	2.076
6	2.560	2.692	2.460	2.231	2.149
7	2.581	2.752	2.498	2.254	2.166
8	2.577	2.775	2.512	2.260	2.168
9	2.609	2.740	2.488	2.244	2.165
10	2.506	2.694	2.473	2.237	2.153
11	2.502	2.665	2.491	2.257	2.172
12	2.614	2.659	2.512	2.297	2.220
13	2.554	2.670	2.569	2.391	2.301
14	2.540	2.681	2.604	2.447	2.369
15	2.534	2.648	2.602	2.461	2.405
16	2.518	2.614	2.596	2.472	2.424
17	2.604	2.612	2.599	2.522	2.510
18	2.658	2.693	2.669	2.651	2.692
19	2.808	2.856	2.835	2.820	2.864
20	2.967	3.007	3.005	3.004	3.059
21	3.140	3.142	3.209	3.247	3.348

Table 4. Level Average: Along Coast Flow.
Defined as in Table 2.

Level	f00	f03	f06	f09	f12
1	2.126	1.926	1.768	1.674	1.675
2	2.149	2.106	1.942	1.823	1.855
3	2.316	2.297	2.082	1.949	1.960
4	2.388	2.481	2.233	2.088	2.086
5	2.482	2.597	2.344	2.184	2.172
6	2.518	2.645	2.398	2.229	2.207
7	2.520	2.657	2.411	2.234	2.210
8	2.521	2.674	2.424	2.238	2.214
9	2.551	2.657	2.437	2.243	2.226
10	2.444	2.628	2.440	2.245	2.233
11	2.449	2.618	2.441	2.255	2.234
12	2.529	2.628	2.459	2.272	2.254
13	2.521	2.652	2.510	2.329	2.306
14	2.525	2.652	2.551	2.379	2.348
15	2.510	2.636	2.574	2.412	2.371
16	2.498	2.639	2.605	2.461	2.409
17	2.595	2.709	2.706	2.585	2.549
18	2.699	2.810	2.825	2.747	2.761
19	2.906	2.995	2.982	2.949	2.994
20	3.140	3.224	3.178	3.178	3.249
21	3.407	3.467	3.411	3.452	3.505

Table 5. Level Average: Offshore Flow.
Defined as in Table 2.

Level	f00	f03	f06	f09	f12
1	2.061	1.872	1.771	1.723	1.713
2	2.021	1.932	1.941	1.942	1.834
3	2.265	2.079	2.061	2.066	1.968
4	2.310	2.254	2.181	2.209	2.133
5	2.402	2.375	2.267	2.292	2.263
6	2.455	2.423	2.297	2.302	2.301
7	2.450	2.429	2.288	2.259	2.273
8	2.460	2.432	2.291	2.229	2.246
9	2.509	2.421	2.257	2.150	2.179
10	2.420	2.428	2.253	2.102	2.130
11	2.415	2.473	2.291	2.135	2.148
12	2.456	2.554	2.380	2.218	2.229
13	2.470	2.607	2.488	2.335	2.340
14	2.517	2.635	2.565	2.435	2.417
15	2.523	2.619	2.599	2.488	2.447
16	2.504	2.597	2.623	2.529	2.470
17	2.646	2.644	2.675	2.650	2.582
18	2.736	2.780	2.812	2.842	2.793
19	2.881	2.963	2.992	3.032	3.019
20	3.012	3.087	3.107	3.168	3.217
21	3.102	3.128	3.193	3.296	3.368

Table 6. Level Average: Onshore Flow.
Defined as in Table 2.

Level	f00	f03	f06	f09	f12
1	2.149	1.973	1.759	1.672	1.671
2	2.091	2.067	1.873	1.800	1.825
3	2.257	2.270	2.017	1.892	1.916
4	2.427	2.492	2.173	2.005	2.040
5	2.546	2.657	2.281	2.070	2.089
6	2.588	2.717	2.325	2.090	2.069
7	2.595	2.720	2.331	2.090	2.056
8	2.638	2.723	2.347	2.102	2.064
9	2.710	2.675	2.387	2.123	2.054
10	2.571	2.658	2.394	2.128	2.064
11	2.501	2.643	2.372	2.120	2.077
12	2.478	2.614	2.351	2.123	2.088
13	2.421	2.583	2.399	2.197	2.140
14	2.423	2.537	2.442	2.259	2.166
15	2.390	2.496	2.468	2.265	2.162
16	2.362	2.477	2.508	2.290	2.189
17	2.413	2.522	2.589	2.477	2.325
18	2.483	2.612	2.710	2.682	2.571
19	2.639	2.759	2.883	2.892	2.870
20	2.749	2.873	3.004	3.036	3.068
21	2.885	2.964	3.048	3.120	3.187

Table 7. Level Average: Weak Flow.
Defined as in Table 2.

APPENDIX B. FIGURES

The following pages of figures are grouped together in this appendix in order to help in the reading of this work.

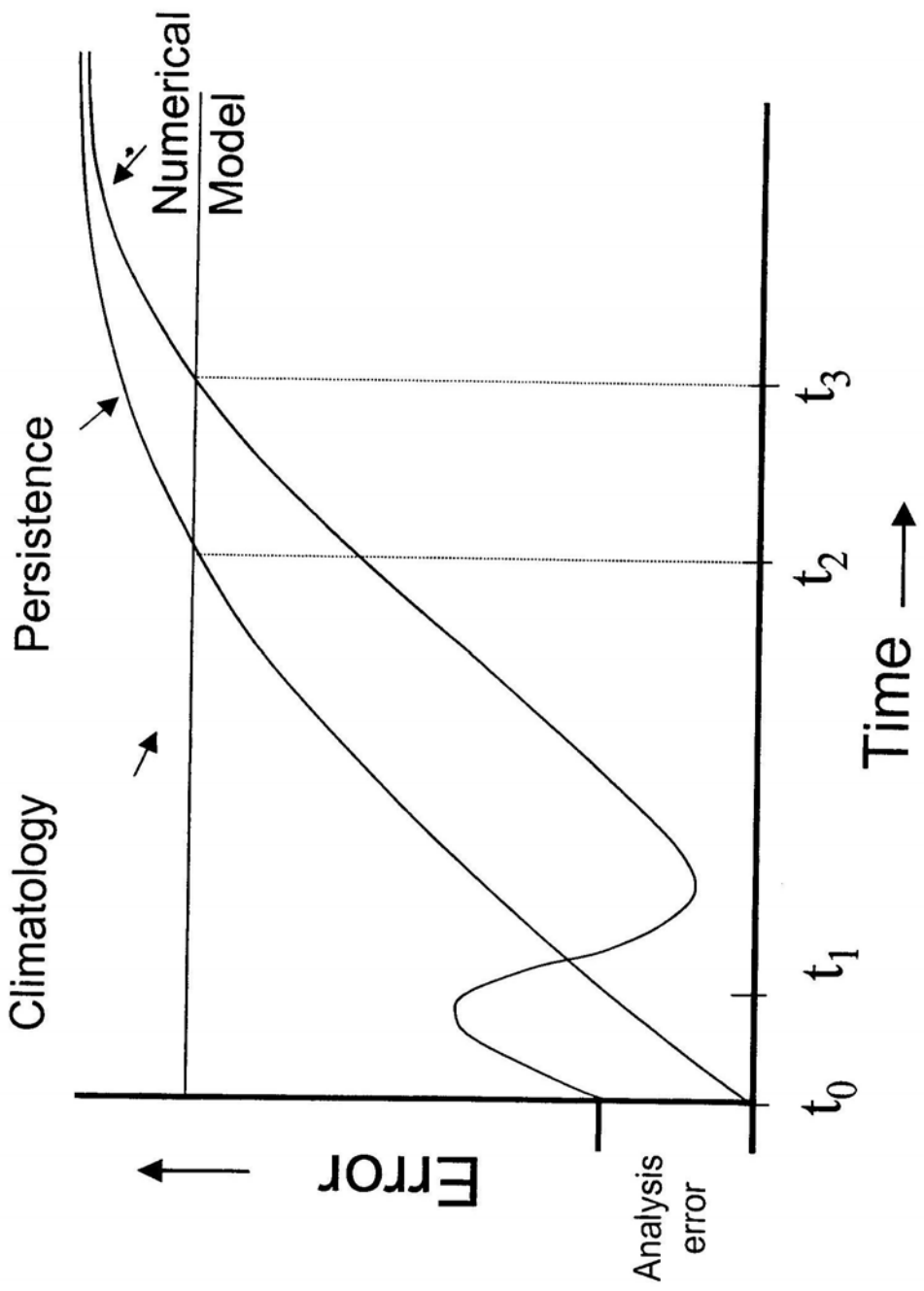

Figure 1: Theoretical Error Growth Curves. (From: Kuypers 2000)

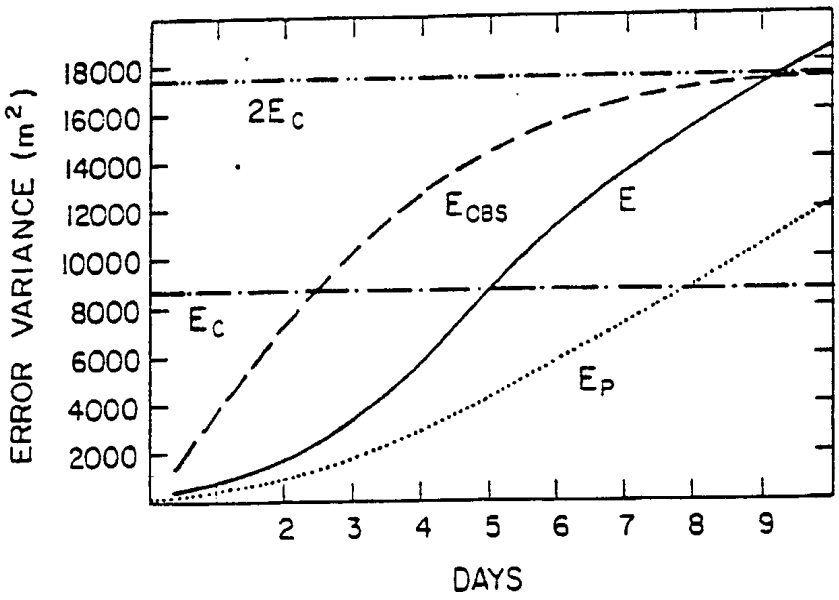

Figure 2. Growth of Error Variance. (From: Anthes 1986)

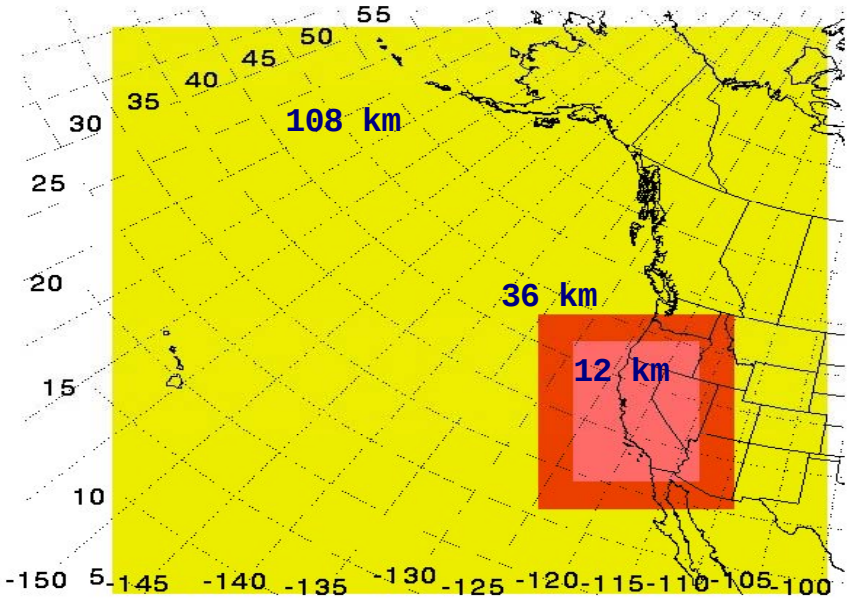

Figure 3. Model nested grid and domain sizes. (From: Miller 2003)

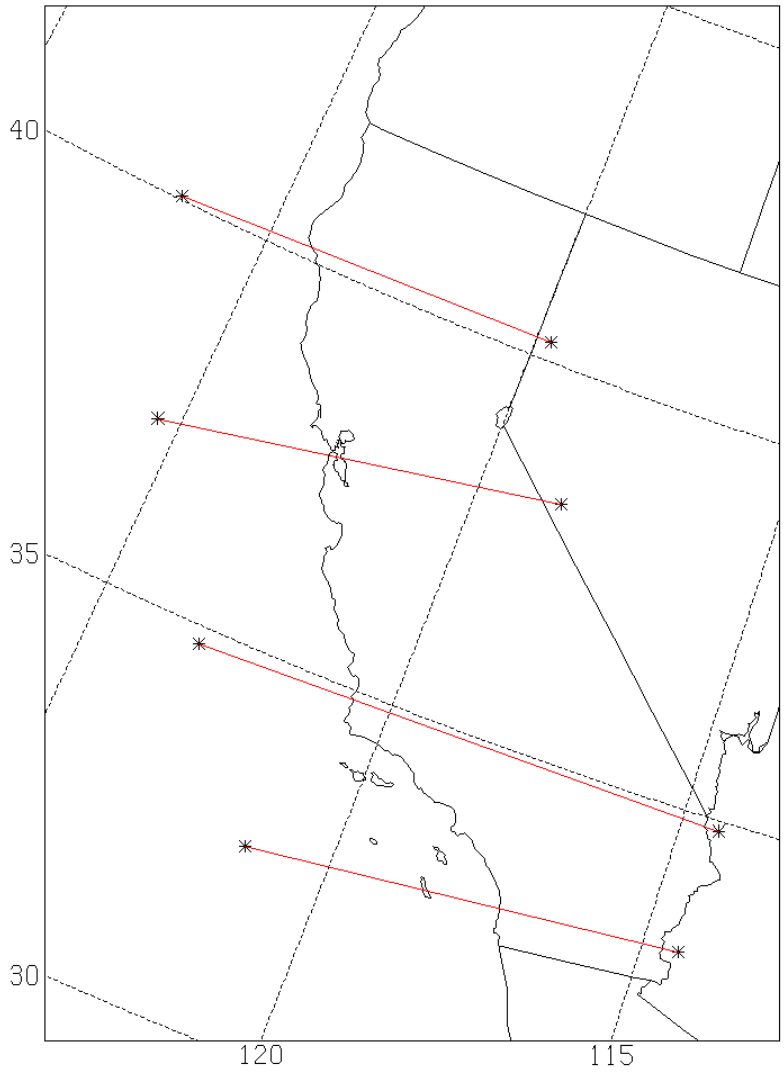

Figure 4. Cross Section Plot.

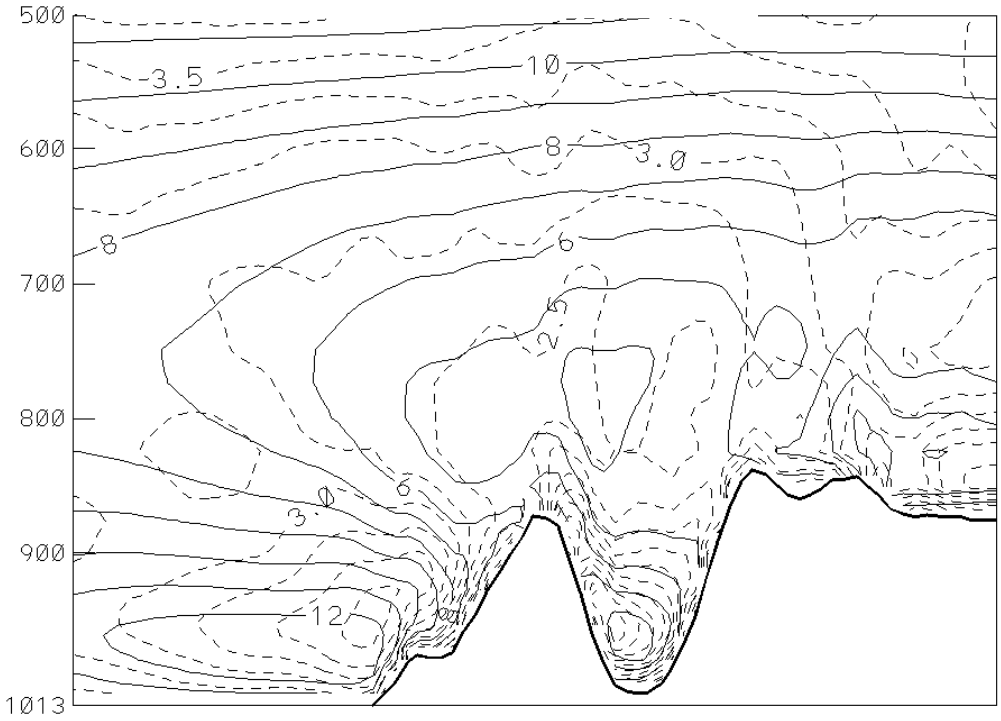

Figure 5. Northern California Cross Section: 00z f03. Mean wind speed in m/s (solid) and spread in m/s (dashed).

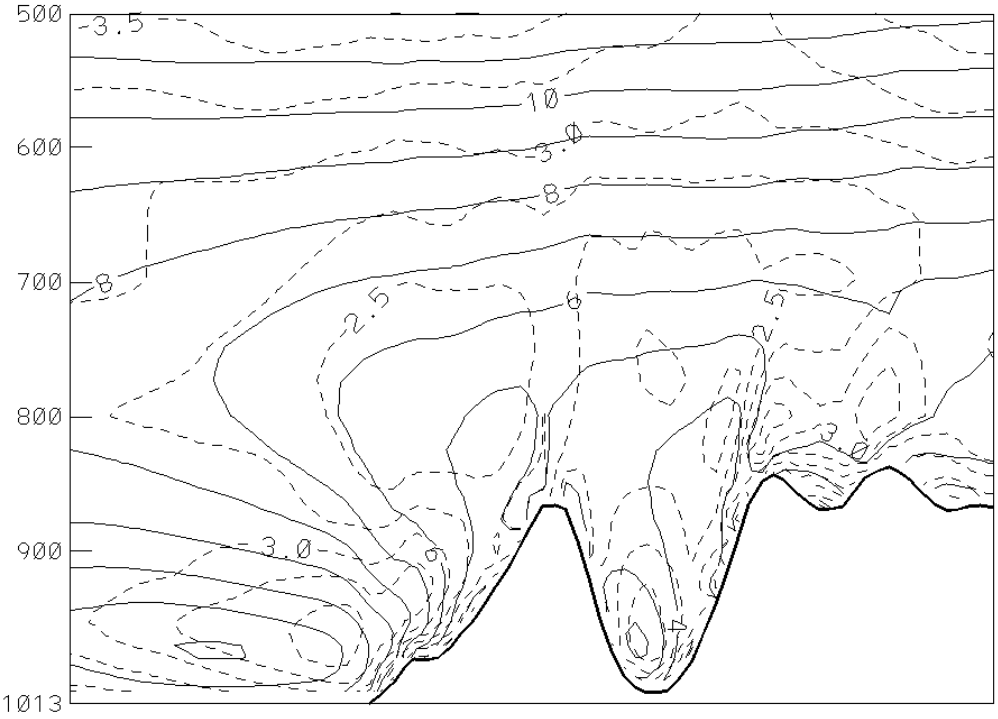

Figure 6. Northern California Cross Section: 12z f03. Mean wind speed in m/s (solid) and spread in m/s (dashed).

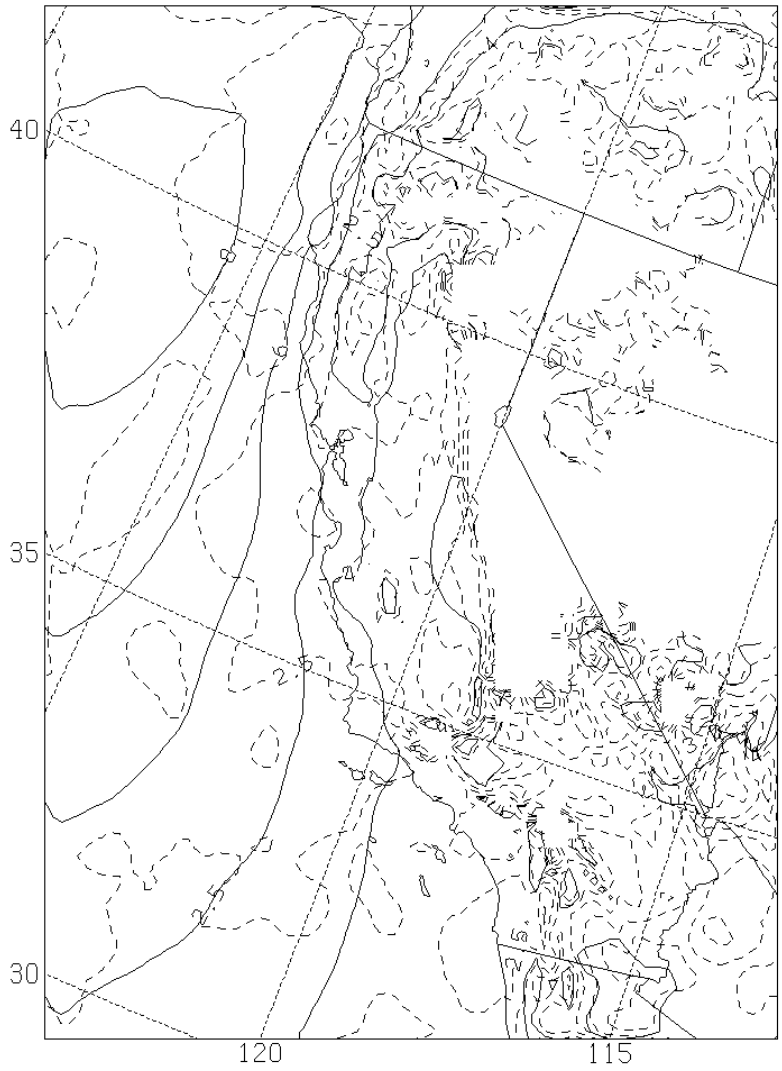

Figure 7. 850mb: 12z f06.
Mean wind speed in m/s (solid) and spread in m/s (dashed).

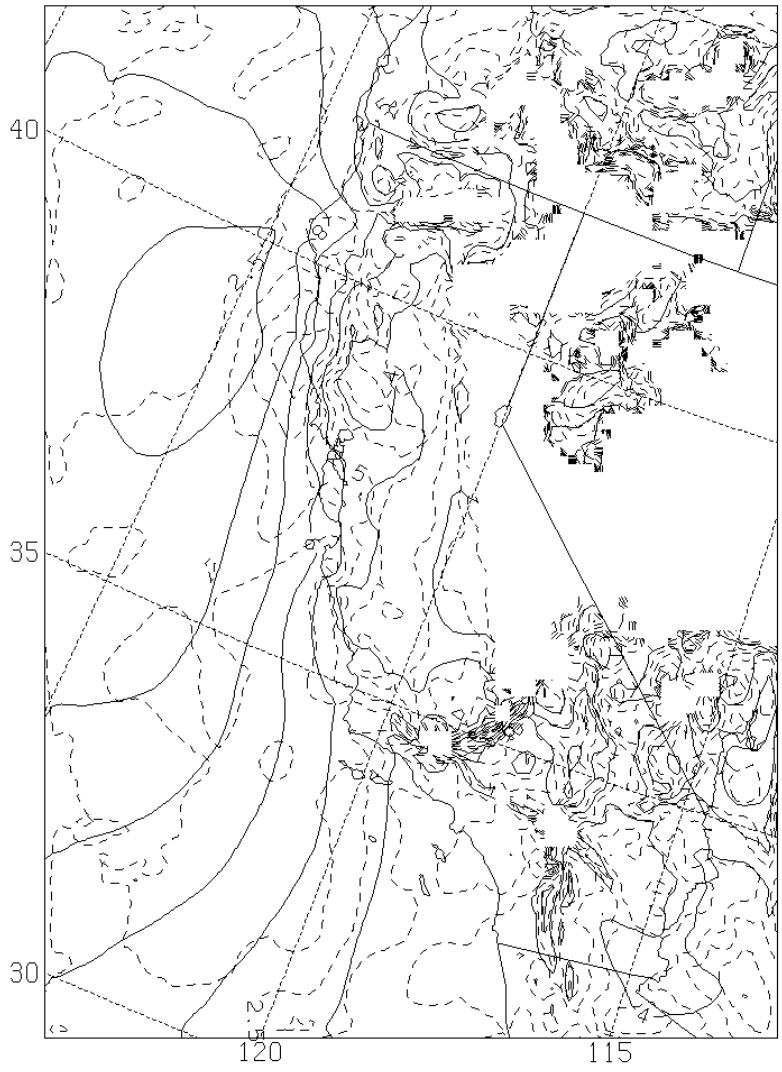

Figure 8. 850mb: Along Coast Flow f06.
Mean wind speed in m/s (solid) and spread in m/s (dashed).

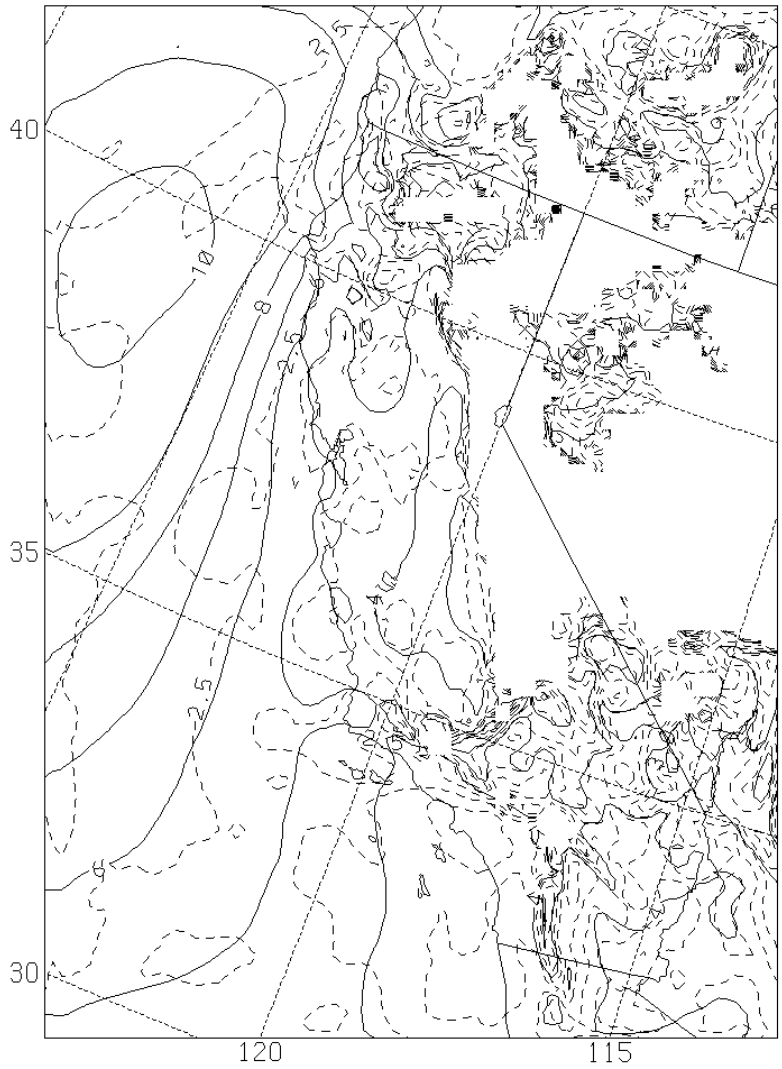

Figure 9. 850mb: Offshore Flow f06.
Mean wind speed in m/s (solid) and spread in m/s (dashed).

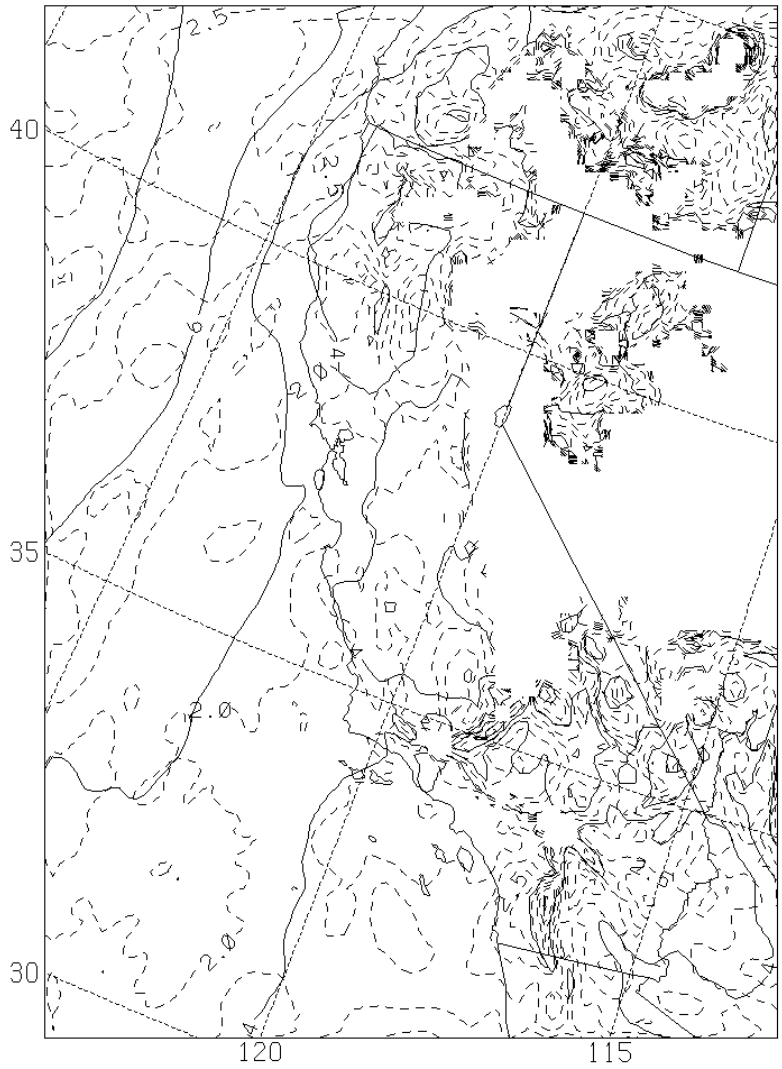

Figure 10. 850mb: Onshore Flow f06.
Mean wind speed in m/s (solid) and spread in m/s (dashed).

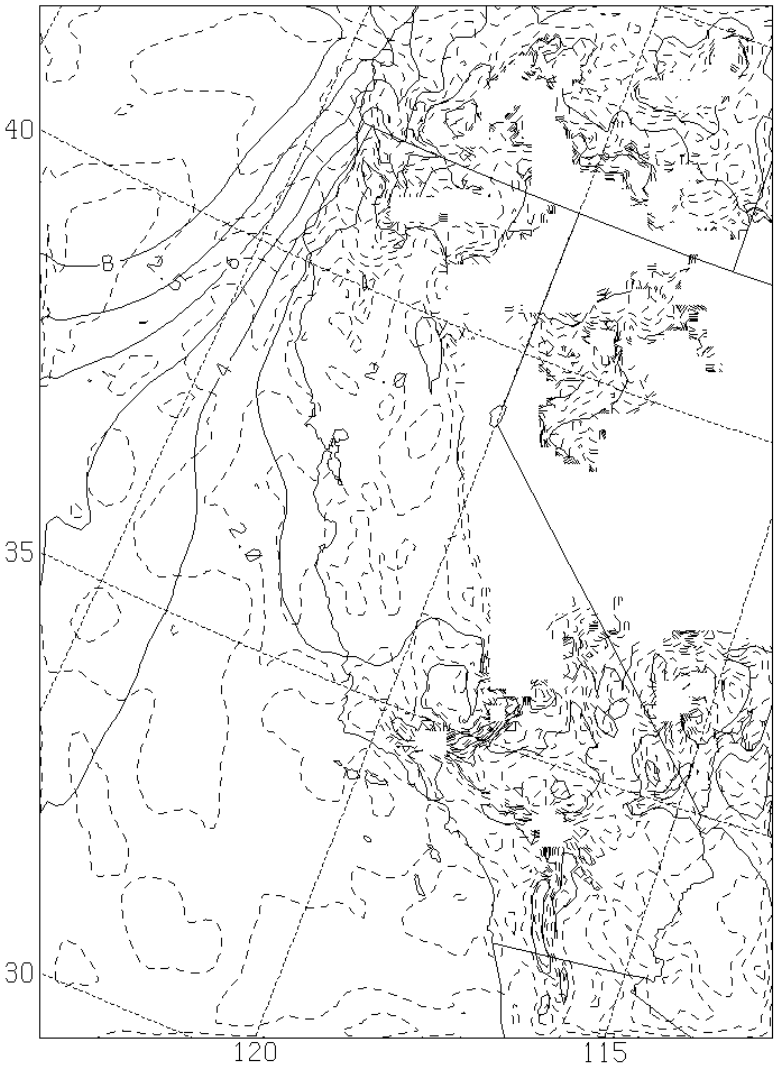

Figure 11. 850mb: Weak Flow f06.
Mean wind speed in m/s (solid) and spread in m/s (dashed).

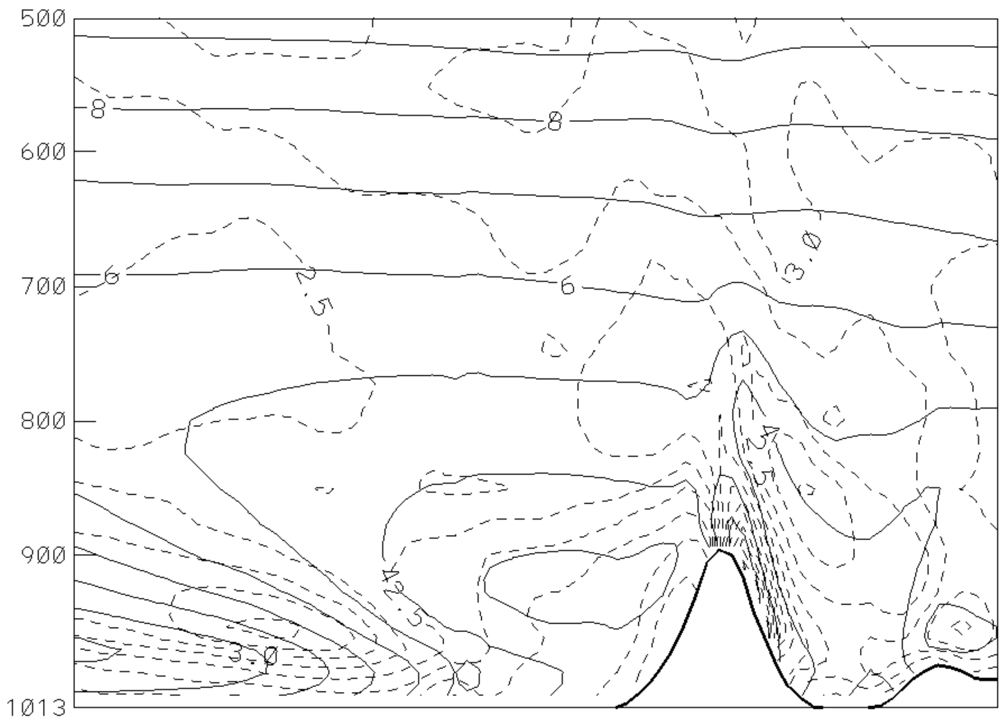

Figure 12. Southern California Cross Section:
Along Coast Flow f00.
Mean wind speed in m/s (solid) and spread in m/s
(dashed).

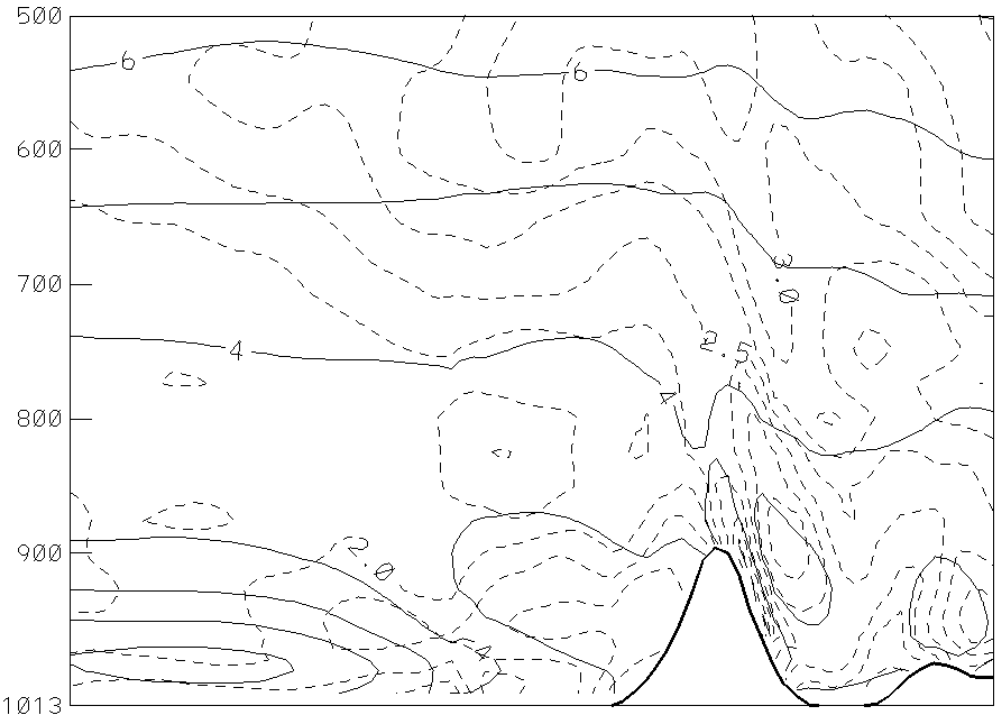

Figure 13. Southern California Cross Section:
Weak Flow f06.
Mean wind speed in m/s (solid) and spread in m/s (dashed).

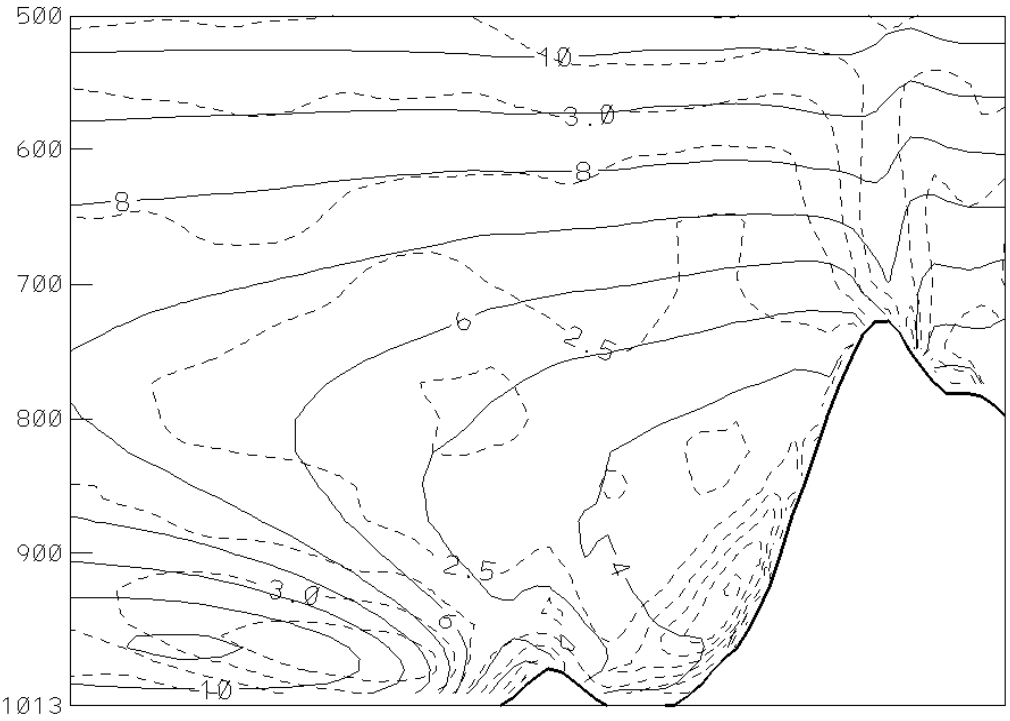

Figure 14. Central California Cross Section: 12z f03. Mean wind speed in m/s (solid) and spread in m/s (dashed).

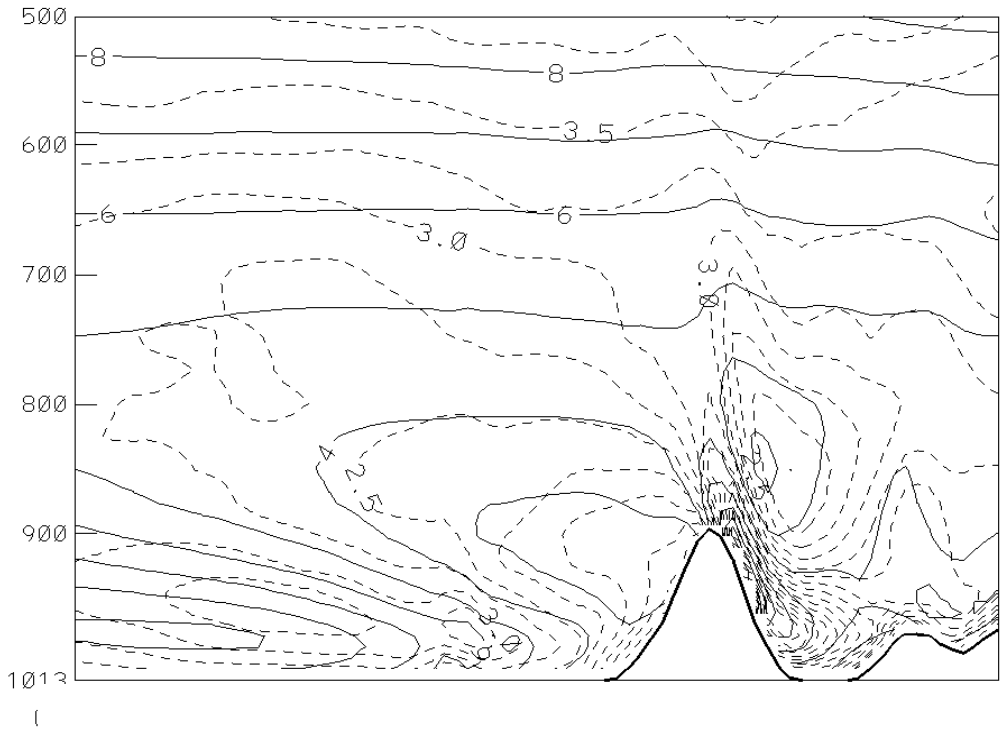

Figure 15. Southern California Cross Section: 00z f03. Mean wind speed in m/s (solid) and spread in m/s (dashed).

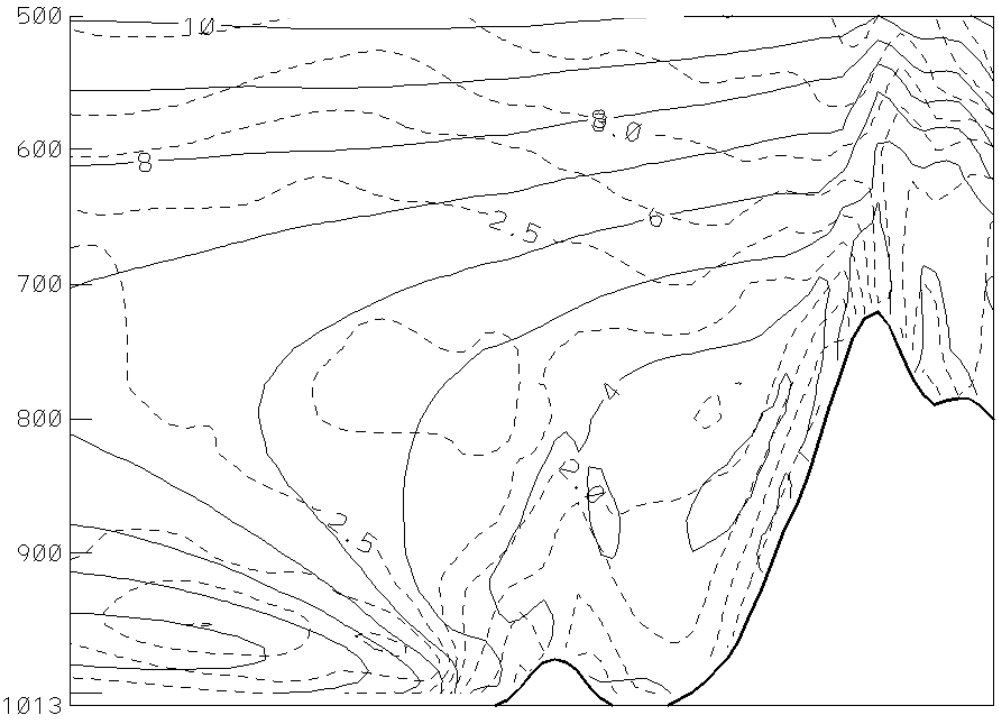

Figure 16. Central California Cross Section: 12z f09. Mean wind speed in m/s (solid) and spread in m/s (dashed).

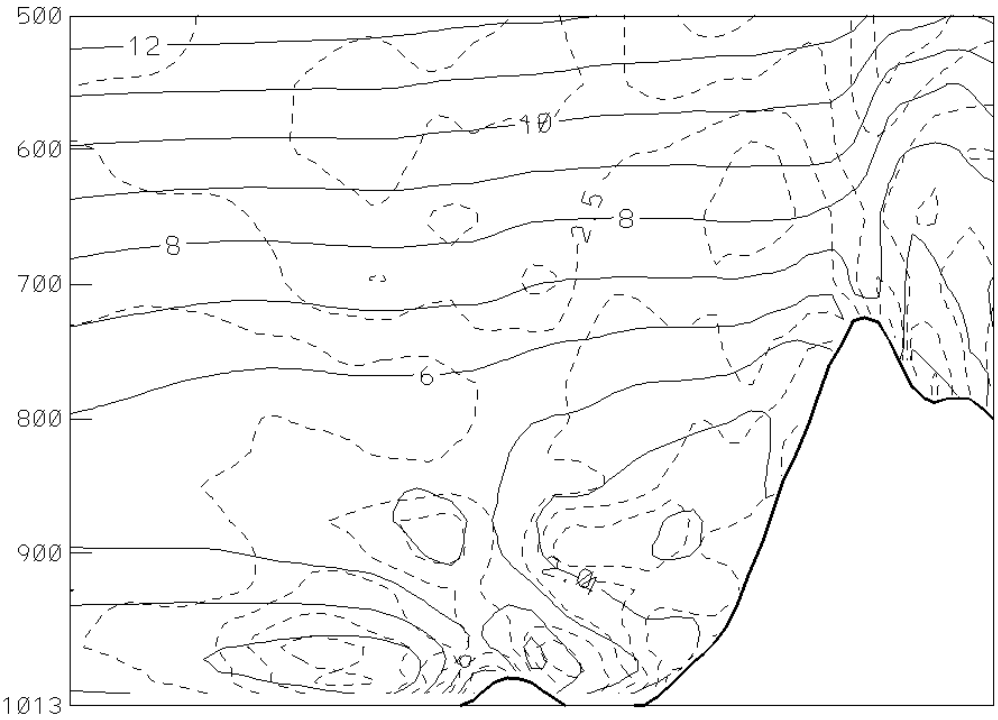

Figure 17. Central California Cross Section:
Onshore Flow f00.
Mean wind speed in m/s (solid) and spread in m/s (dashed).

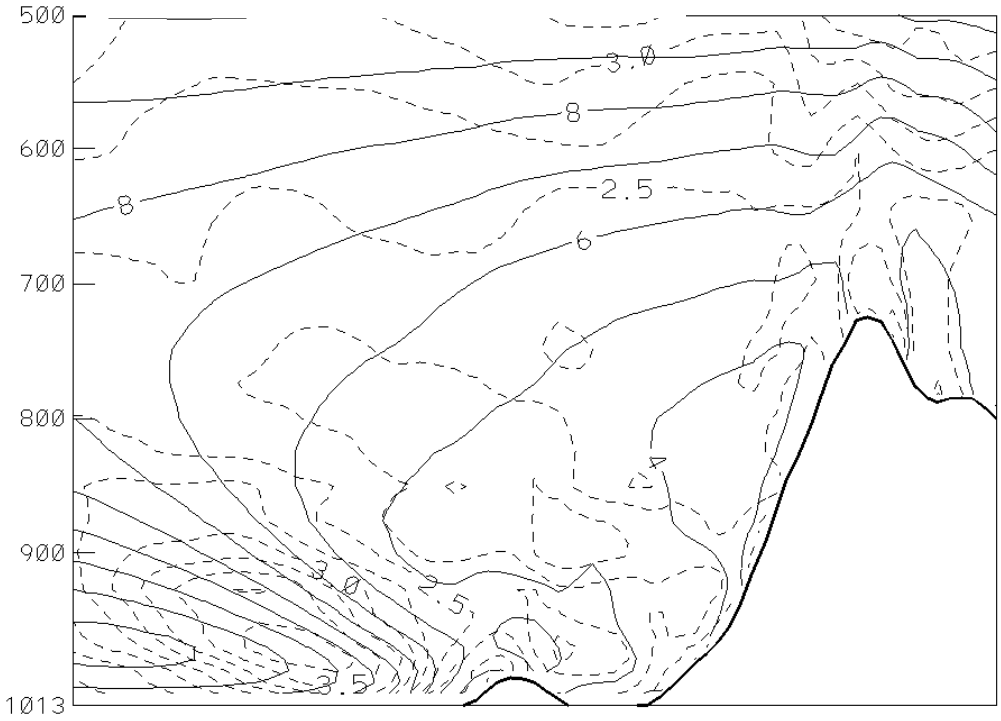

Figure 18. Central California Cross Section:
Offshore Flow f00.
Mean wind speed in m/s (solid) and spread in m/s (dashed).

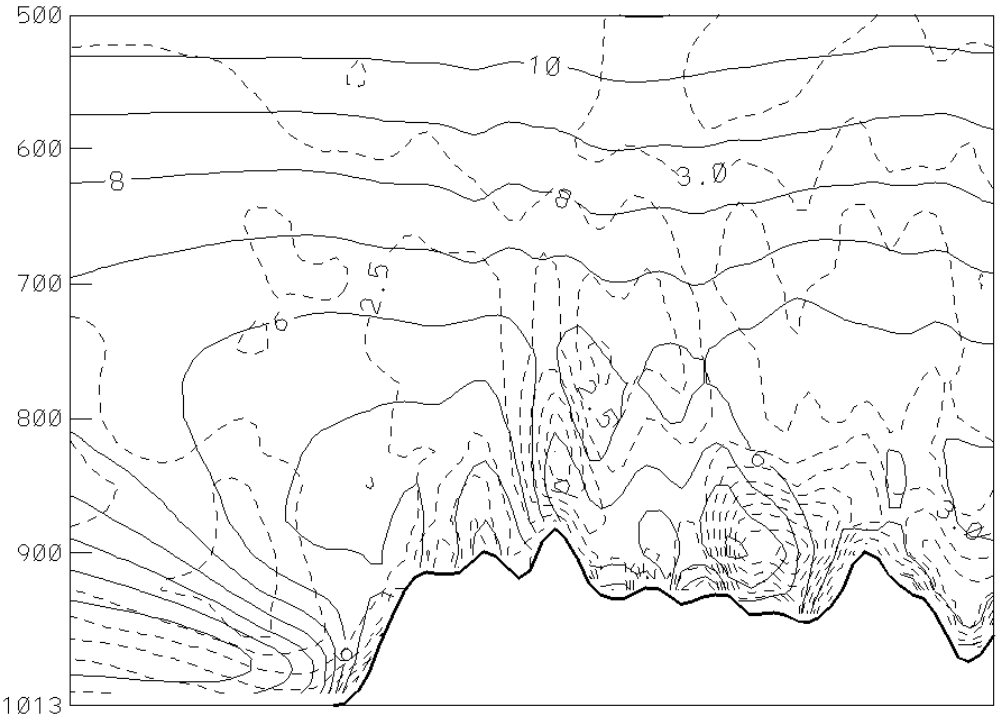

Figure 19. Point Conception Cross Section:
Along Coast Flow f03.
Mean wind speed in m/s (solid) and spread in m/s (dashed).

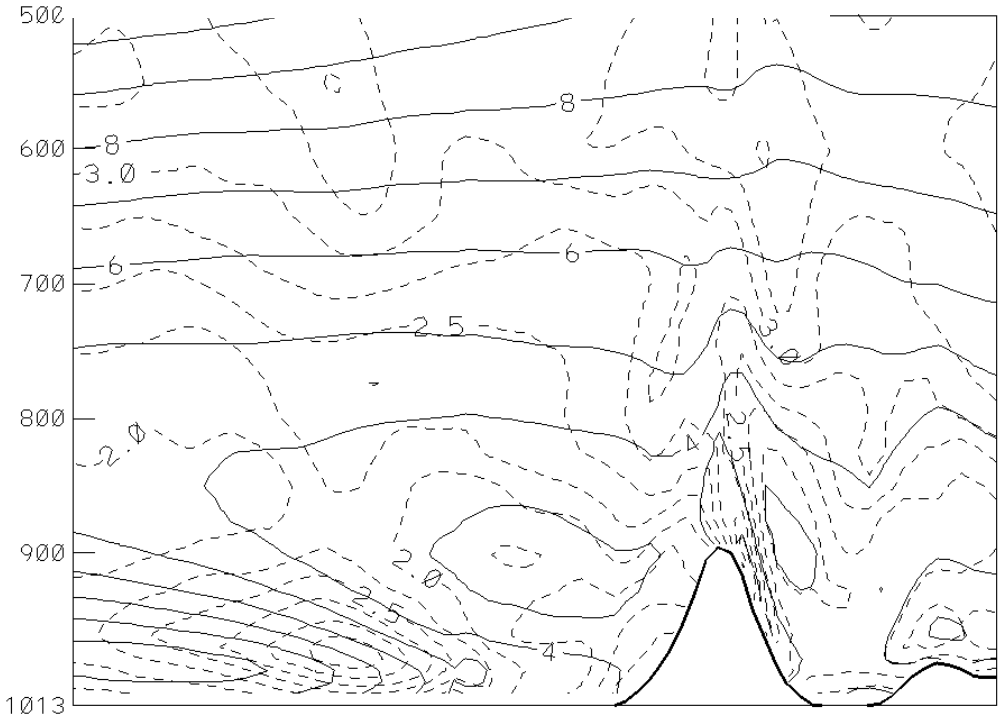

Figure 20. Southern California Cross Section:
Onshore Flow f09.
Mean wind speed in m/s (solid) and spread in m/s (dashed).

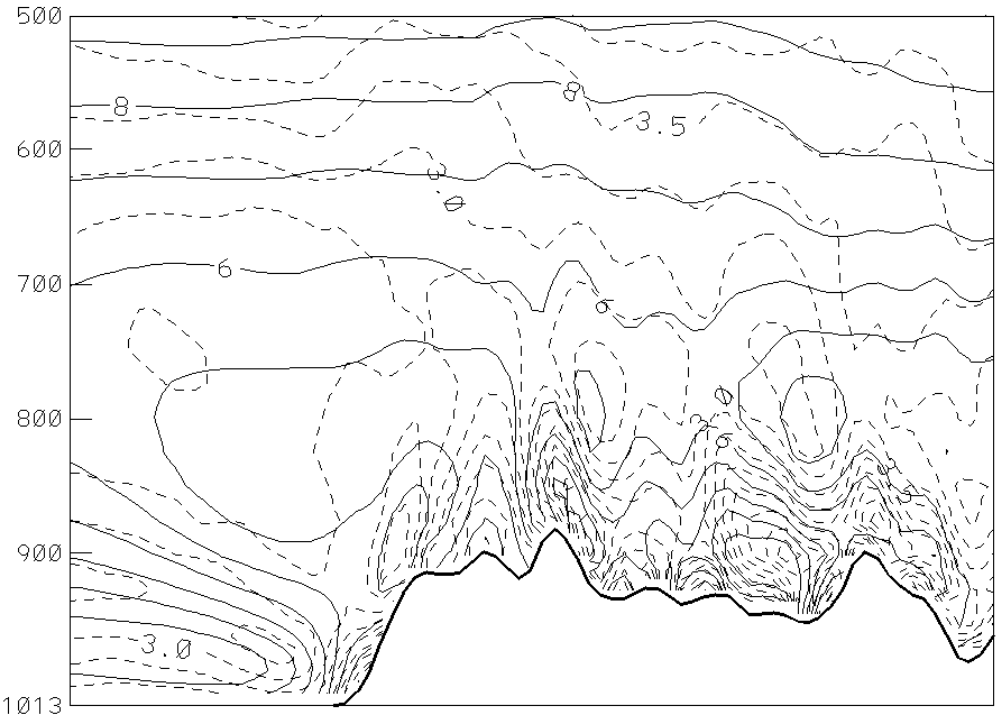

Figure 21. Point Conception Cross Section: 00z f06. Mean wind speed in m/s (solid) and spread in m/s (dashed).

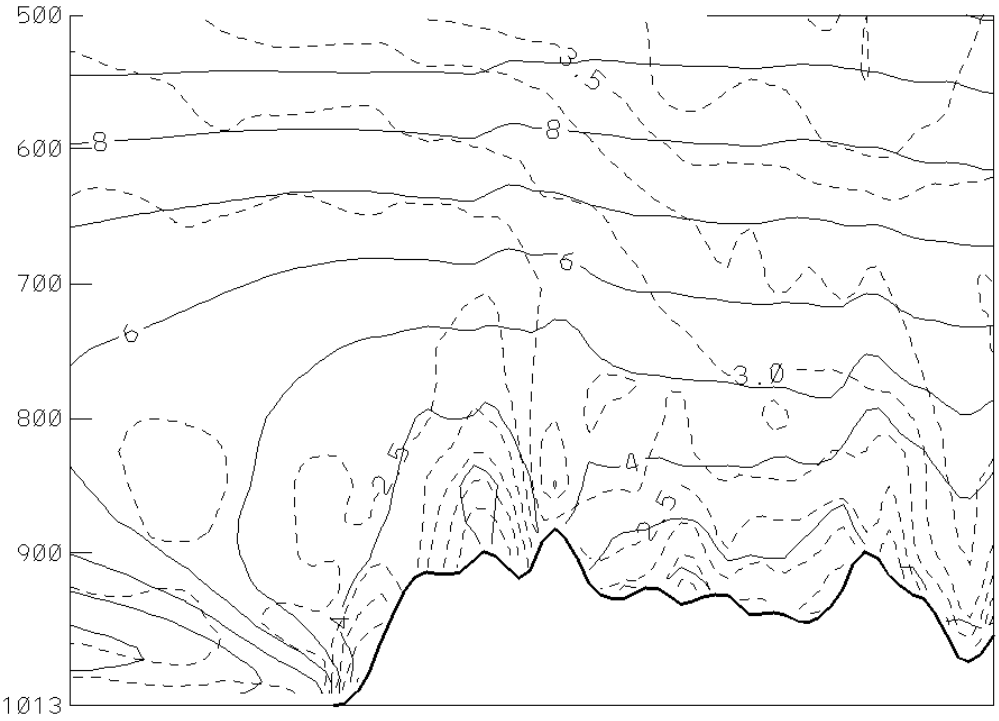

Figure 22. Point Conception Cross Section: 12z f06. Mean wind speed in m/s (solid) and spread in m/s (dashed).

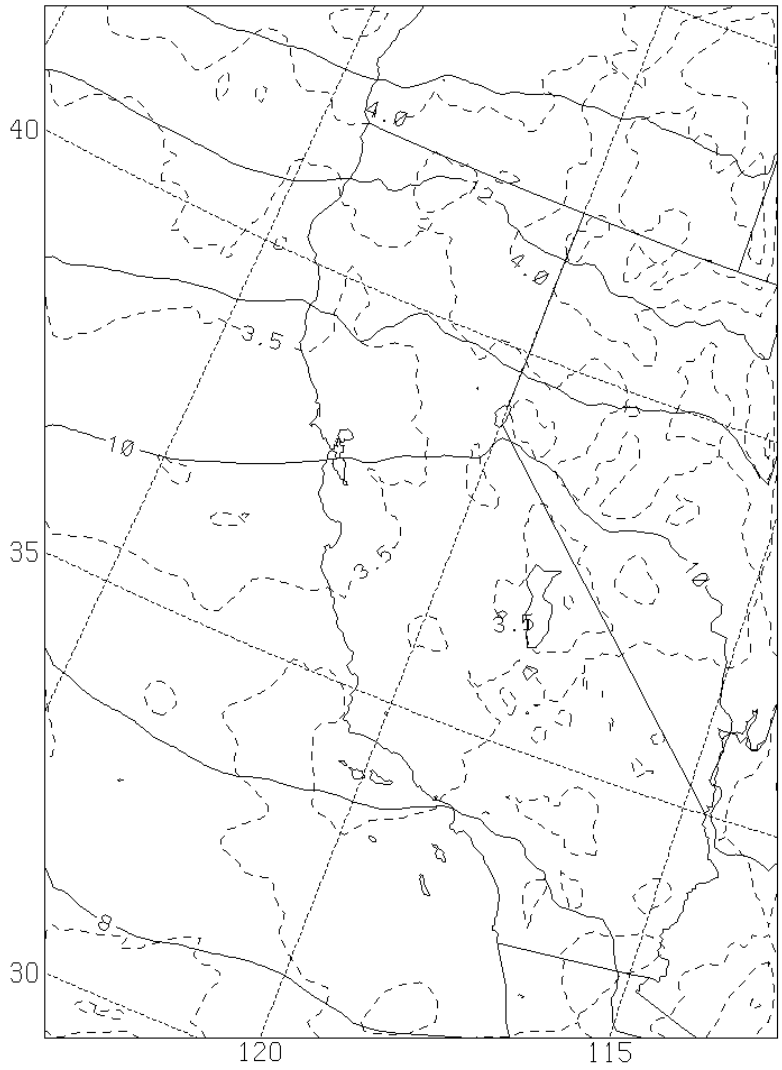

Figure 23. 500mb: 00z f06.
Mean wind speed in m/s (solid) and spread in m/s (dashed).

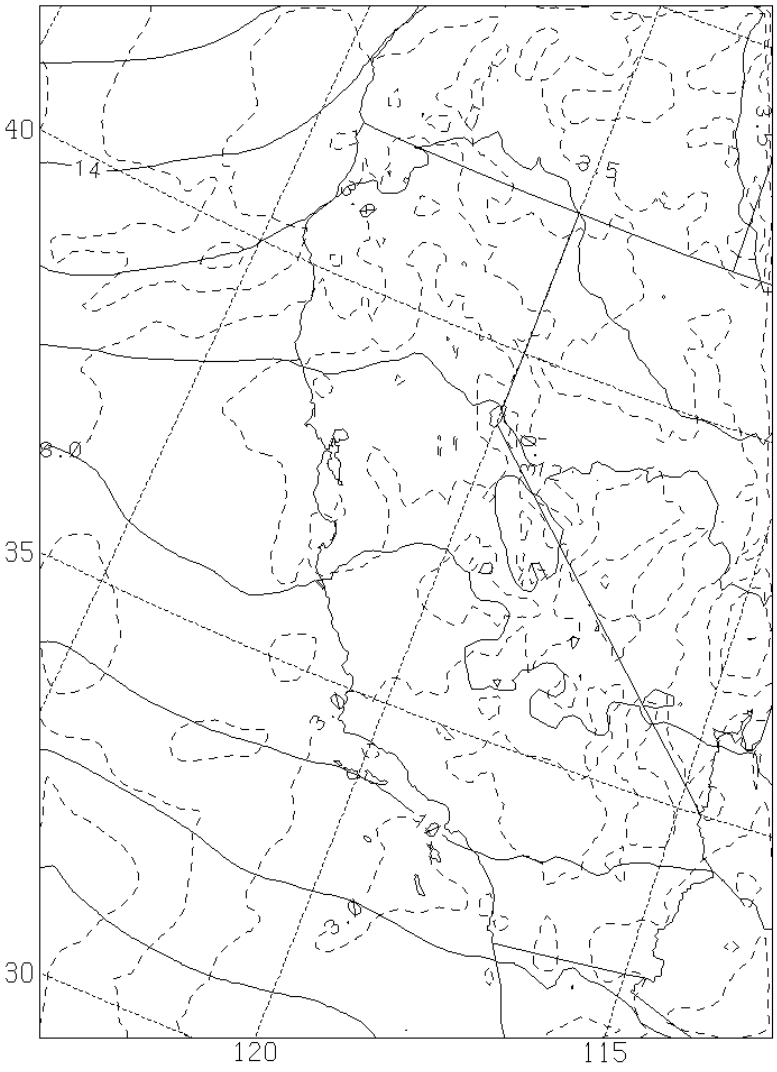

Figure 24. 500mb: Along Coast Flow f00.
Mean wind speed in m/s (solid) and spread in m/s (dashed).

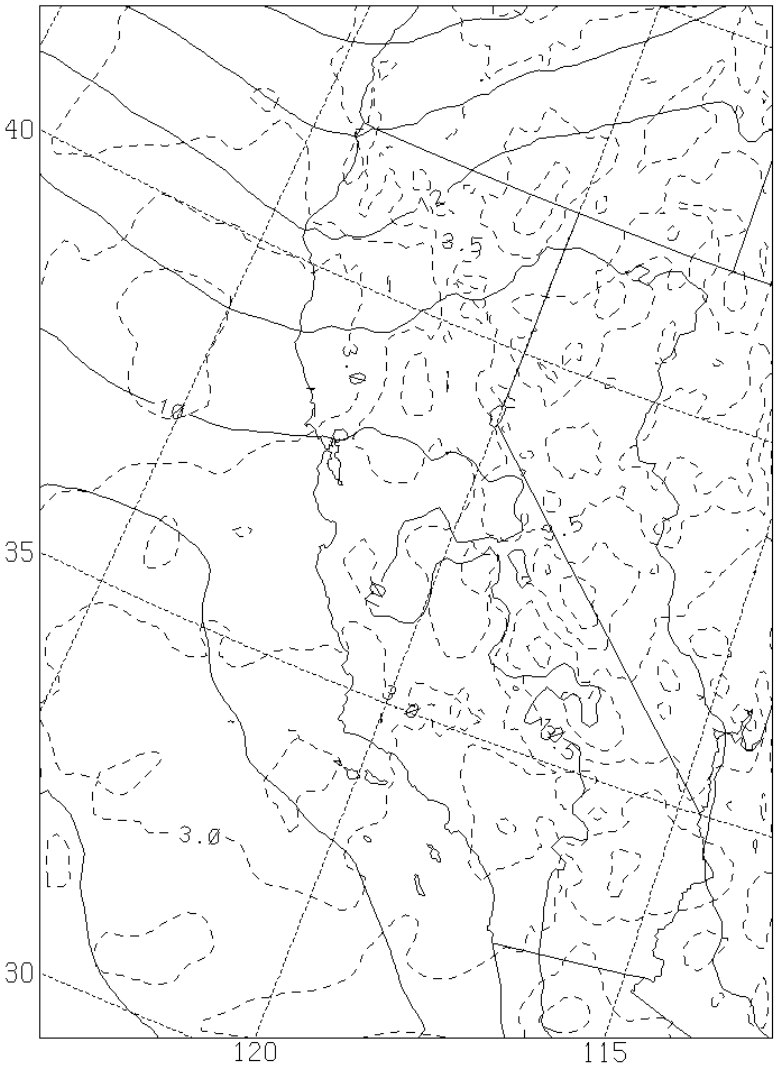

Figure 25. 500mb: Offshore Flow f00.
Mean wind speed in m/s (solid) and spread in m/s (dashed).

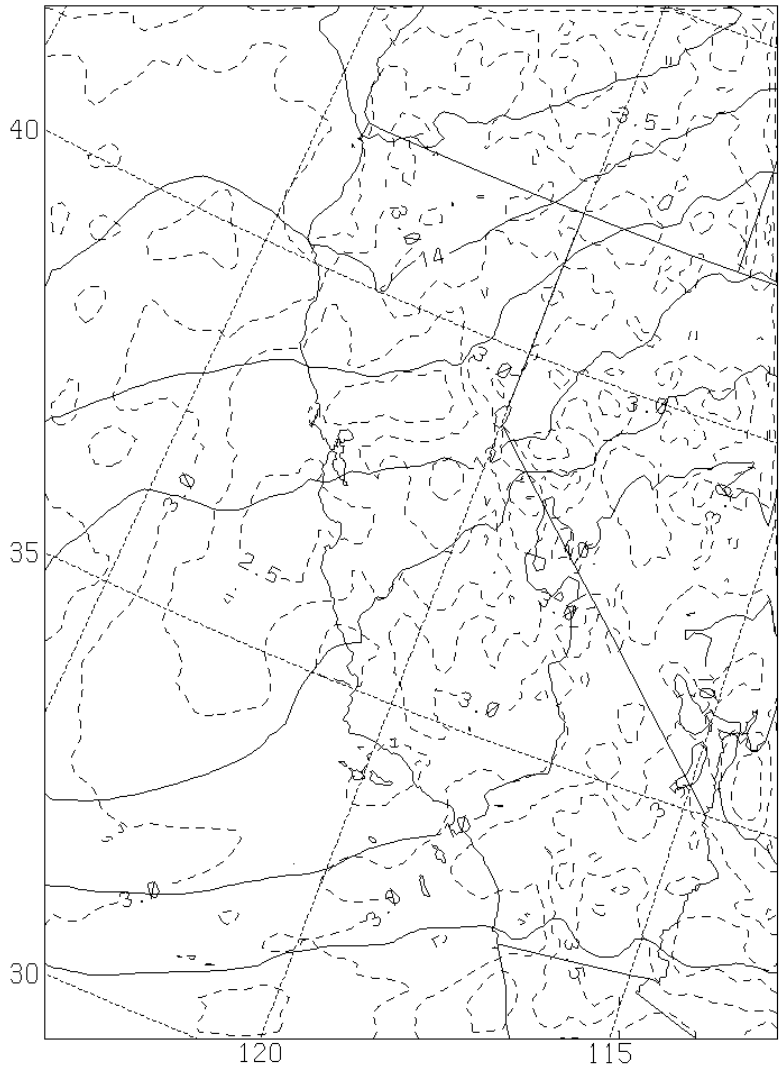

Figure 26. 500mb: Onshore Flow f00.
Mean wind speed in m/s (solid) and spread in m/s (dashed).

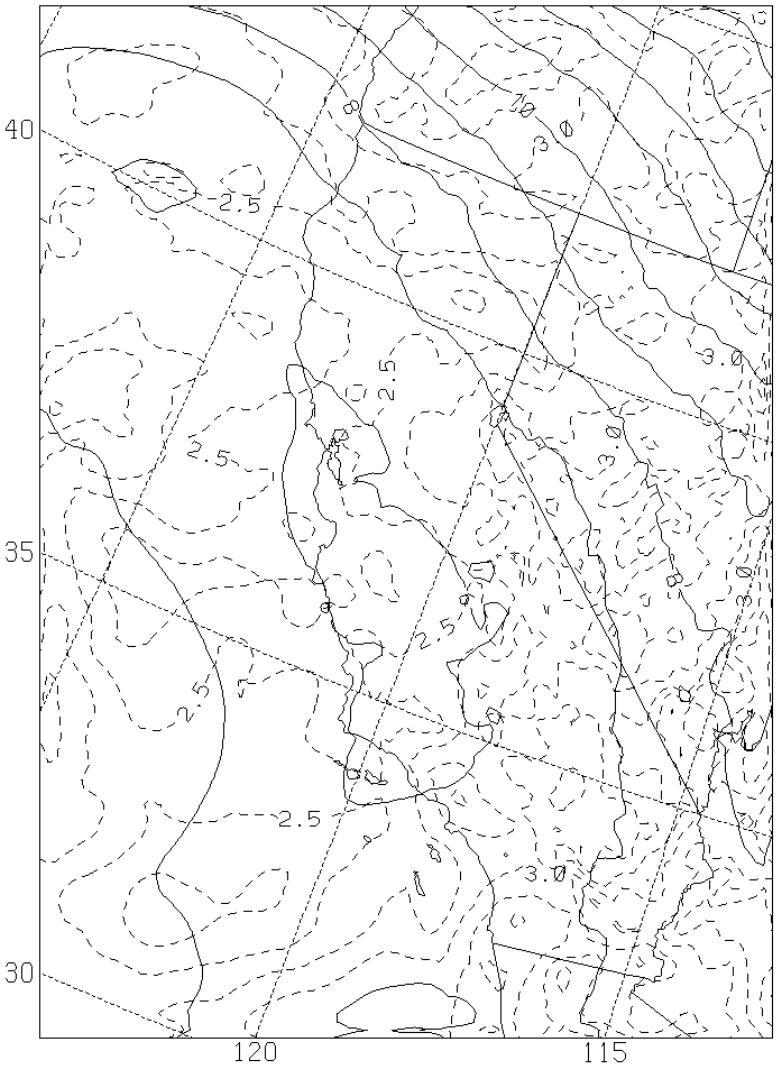

Figure 27. 500mb: Weak Flow f00.
Mean wind speed in m/s (solid) and spread in m/s (dashed).

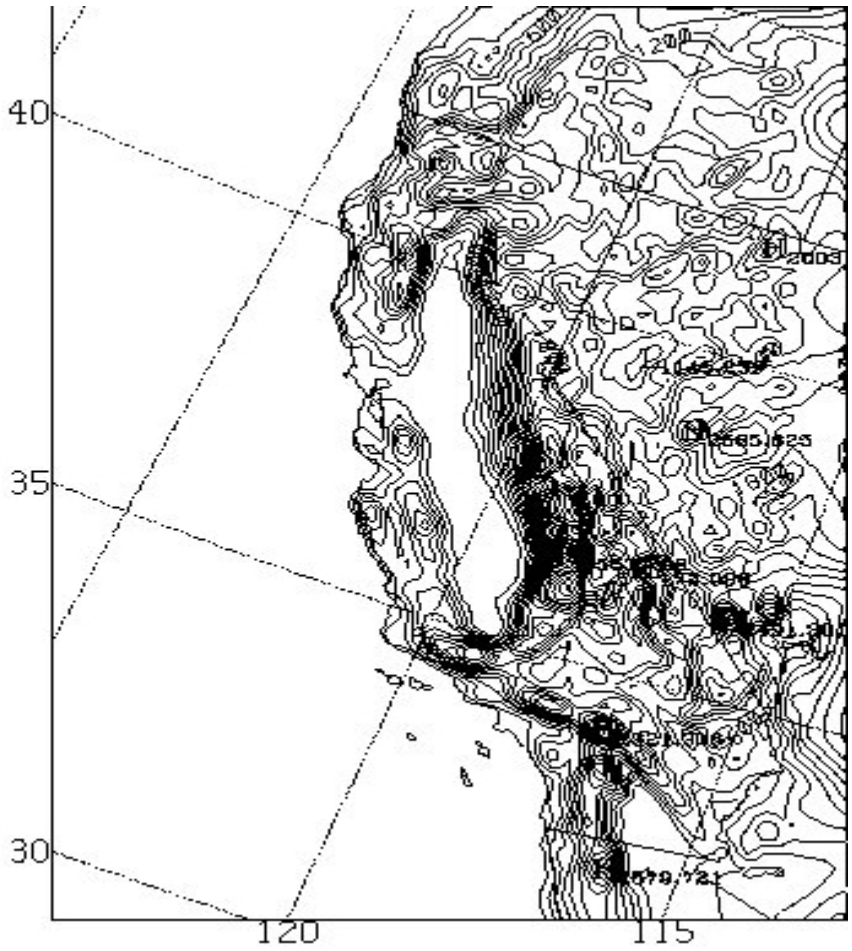

Figure 28. Model Topography. (From: Miller 2003)

LIST OF REFERENCES

Ahrens, C.D., 1994: *Meteorology Today: An Introduction to Weather, Climate, and the Environment.* West Publishing Co.,560pp.

Anthes, R.A., 1986: The General Question of Predictability. *Mesoscale Meteorology and Forecasting*, P.S. Ray (Ed.), Amer. Meteor. Soc., 636-655.

Anthes, R.A., and D.P. Baumhefner, 1984: A diagram depicting forecast skill and predictability. *Bull. Amer. Meteor. Soc.*, **65**, 701-703.

COMET 2003: *Mesoscale Meteorology*. [http://www.meted.ucar.edu/].

Durran, D.R., 1986: Mountain Waves. In: *Mesoscale Meteorology and Forecasting*, P.S. Ray, Ed., Am Meteor. Soc., 472-492.

Doyle, J.D, 1997: The influence of mesoscale orography on a coastal jet and rainband*. Mon. Wea. Rev.*, **125**, 1465-1488.

Grell, G.A., J. Dudhia and D.R. Stauffer, 1994: A description of the fifth-generation Penn State/NCAR mesoscale model (MM5). *NCAR Technical Note*, NCAR/TN-398+STR, 117pp.

Kuypers, M.A., 2000: *Understanding Mesoscale Error Growth And Predictability*, Master's Thesis, Naval Postgraduate School, Monterey, California, September 2000.

Lorenz, E.N., 1965: A study of the predictability of a 28-variable atmospheric model. *Tellus*, **17**, 321-333.

-----, 1969: The predictability of a flow which possesses many scales of motion. *Tellus*, **21**, 289-307.

-----, 1982: Atmospheric predictability experiments with a large numerical model. *Tellus*, **36A**, 505-513.

Mass, C.F., D. Owens, K. Westrick, and B.A. Colle, 2002: Does increasing horizontal resolution produce more skillful forecasts? *Bull. Amer. Meteor. Soc.*, **83**, 407-430.

Miller, D.K. *Model Setup Information*. [http://www.weather.nps.navy.mil/~dkmiller/MM5/]. 27 December 2002.

Monterrosa, O.E., 1999: *Comparison of TAMS/RT Surface Wind, Temperature, and Pressure Fields with Surface Observations and Model Analyses in the SOCAL Area*, Master's Thesis, Naval Postgraduate School, Monterey, California, December 1999.

Nuss, W.A., 2002: *Coastal Meteorology*: *Course Notes for MR4240*. Department of Meteorology, Naval Postgraduate School, Monterey, California. 68pp.

-----, and S. Drake, 1995: *VISUAL Meteorological Diagnostic and Diplay Program*. 51 pp.

-----, and D.K. Miller, 2001: Mesoscale predictability under various synoptic regimes. *Nonlinear Processes in Geophysics*, **19**, 1-10.

PSU/NCAR, *MM5 Home Page*. [http://www.mmm.ucar.edu/mm5/mm5-home.html]. 11 February 2003.

Steenburgh, W.J., 2002: Using real-time mesoscale modeling in undergraduate education. *Bull. Amer. Meteor. Soc.*, **83**, 1447-1451.

Tennekes, H. 1978: Turbulent flow in two and three dimensions. *Bull. Amer. Meteor. Soc*., **59**, 22-28.

UCAR, 1998: *GEMPAK fact sheet*. [http://www.unidata.ucar.edu/factsheet.html]. 20 March 2003.

Weygandt, S.S., and Seaman, N.L. 1994: Quantification of predictive skill for mesoscale and synoptic-scale meteorological features as a function of horizontal grid resolution. *Mon. Wea. Rev.*, **122**, 57-71.

INITIAL DISTRIBUTION LIST

1. Defense Technical Information Center
   Ft. Belvoir, VA

2. Dudley Knox Library
   Naval Postgraduate School
   Monterey, CA

3. Chairman, Code MR/Wx
   Department of Meteorology
   Naval Postgraduate School
   Monterey, CA

4. Chairman, Code OC/Bv
   Department of Oceanography
   Naval Postgraduate School
   Monterey, CA

5. Dr. Wendell A. Nuss, Code MR/Nu
   Department of Meteorology
   Naval Postgraduate School
   Monterey, CA

6. LCDR David S. Brown, Code MR/BD
   Department of Meteorology
   Naval Postgraduate School
   Monterey, CA

7. Dr. Douglas K. Miller, Code Mr/Z
   Department of Meteorology
   Naval Postgraduate School
   Monterey, CA

8. LTjg Jodi C. Beattie
   Carmel, CA